RESEARCH ARTICLE

Neurolin expression in the optic nerve and immunoreactivity of Pax6-positive niches in the brain of rainbow trout (*Oncorhynchus mykiss*) after unilateral eye injury

Evgeniya V. Pushchina[1, 2, *], **Anatoly A. Varaksin**[1]

1 National Scientific Center of Marine Biology, Far Eastern Branch, Russian Academy of Sciences, Vladivostok, Russia
2 A.A. Bogomoletz Institute of Physiology, National Academy of Sciences of Ukraine, Kiev, Ukraine

Funding: *This work was supported by the President of the Russian Federation (grant No. MD-4318.2015.4; to EVP) and by the Far East Branch of the Russian Academy of Sciences within the Program for Basic Research for 2015–2017 (grant No. 15-I-6-116; section III; to AAV and EVP).*

Abstract

In contrast to astrocytes in mammals, fish astrocytes promote axon regeneration after brain injury and actively participate in the regeneration process. Neurolin, a regeneration-associated, Zn8-labeled protein, is involved in the repair of damaged optic nerve in goldfish. At 1 week after unilateral eye injury, the expression of neurolin in the optic nerve and chiasm, and the expression of Pax6 that influences nervous system development in various brain regions in the rainbow trout (*Oncorhynchus mykiss*) were detected. Immunohistochemical staining revealed that the number of $Zn8^+$ cells in the optic nerve head and intraorbital segment was obviously increased, and the increase in $Zn8^+$ cells was also observed in the proximal and distal parts of injured optic nerve. This suggests that $Zn8^+$ astrocytes participate in optic nerve regeneration. ELISA results revealed that Pax6 protein increased obviously at 1 week post-injury. Immunohistochemical staining revealed the appearance of $Pax6^+$ neurogenic niches and a larger number of neural precursor cells, which are mainly from $Pax6^+$ radial glia cells, in the nuclei of the diencephalon and optic tectum of rainbow trout (*Oncorhynchus mykiss*). Taken together, unilateral eye injury can cause optic nerve reaction, and the formation of neurogenic niches is likely a compensation phenomenon during the repair process of optic nerve injury in rainbow trout (*Oncorhynchus mykiss*).

***Correspondence to:**
Evgeniya V. Pushchina, DSci, PhD, puschina@mail.ru.

orcid:
0000-0003-0388-3147 (Evgeniya V. Pushchina)

doi: *10.4103/1673-5374.243721*

Received: *February 23, 2018*
Accepted: *September 6, 2018*

Key Words: *optic nerve injury; neurolin; Zn8; Pax6; rainbow trout (Oncorhynchus mykiss); radial glia cells; microenvironment; neural regeneration*

Chinese Library Classification No. *R459.9; R361; Q2*

Introduction

Regulatory genes of the paired box (PAX) family are key factors that influence the development of the central nervous system (CNS) during embryogenesis, the regionalization of the CNS, cell migration during embryogenesis and postembryonic development, and the switch from cell proliferation to cell differentiation (Thomson and Ziman, 2011). The participation of the PAX family genes in the mechanisms regulating neurodegenerative diseases, neurotrauma, and apoptosis is particularly interesting. In addition to the involvement of Pax6 genes in embryogenesis, a high level of Pax6 expression maintains the phenotypes of progenitor cells in adult animals and the plasticity of mature neurons in response to various environmental stimuli (Gerber et al., 2002). A lack of Pax6 during the postnatal development of astrocytes reduces neurogenic potential (Heins et al., 2002). In addition, Pax6 regulates the survival of dopaminergic periglomerular neurons by inhibiting apoptosis in mature olfactory neurons (Ninkovic et al., 2010).

In contrast to astrocytes in mammals, fish astrocytes promote axon regeneration after brain injury and actively participate in the regenerative process (Garcia and Koke, 2009). Neurolin (a regeneration-associated, Zn8 labeled protein) is involved in repairing the damaged optic nerve in goldfish (Parrilla et al., 2009). Zn8 expression was observed in regenerating axons of the optic nerve in goldfish on days 15 to 30 post-injury (Parrilla et al., 2013). Along with other regeneration factors, in particular, the expression of the transcription factor Pax2 and glutamine synthetase in astrocytes, neurolin expression is associated with the regeneration of optic nerve axons in goldfish (Parrilla et al., 2012, 2013). On days 15 to 30 post-injury, the number of $Pax2^+$ astrocytes in a goldfish decreases to the control level. Immunolabeling for Zn8 in regenerating axons was observed in the growing edge close to the chiasm and in the optic nerve head (ONH) in adult goldfish (Parrilla et al., 2013). $Pax2^+$ astrocytes were located in close proximity to the young $Zn8^+$ axons, similar to intact goldfish (Parrilla et al., 2009). No investigation of the distribution of neurolin in the earlier periods of optic nerve regeneration in fish has been conducted. Astrocytes in the ONH also participate in the guidance and organization of axons after an injury, modifying the expression of axon guidance molecules such as Netrin1 and packing the newly formed axons (Becker and Becker, 2007).

A study of the expression of subunits of the Pax6 transcription factor (Pax6a and Pax6b) in the brain of developing zebrafish embryos, *Danio rerio*, showed that both subunits are expressed in the retina, as well as in the developing telencephalon, diencephalon, and brain stem (Kleinjan et al., 2008). Notably, these genes are expressed in the area of brain neuromeres, as well as at the border of mesencephalic tegmentum and medulla oblongata in zebrafish (Wullimann

and Muller, 2004). Pax6 is expressed at high levels in these areas of the brains of zebrafish and other vertebrates during early embryogenesis (Stoykova and Gruss, 1994; Wullimann and Muller, 2004), but the localization of this transcription factor in later ontogenesis has not yet been studied. The functional implications of Pax6 in the brains of adult vertebrates have received substantially increasing attention after the discovery that this factor is involved in the processes of reparative neurogenesis in vertebrate animals and humans (Thomson and Ziman, 2011). The presence of Pax6 in the periventricular regions of brain in juvenile masu salmon, *Oncorhynchus masou*, is associated with the participation of this factor in the constitutive neurogenesis processes observed in juvenile salmonids (Pushchina et al., 2012). We used the previously obtained immunohistochemical (IHC) data for Pax6 labeling in the telencephalon, diencephalon, and brainstem of yearling masu salmon, *Oncorhynchus masou* (Pushchina et al., 2013) to identify the areas expressing Pax6 in the adult trout brain. In these studies, the Pax6 transcription factor is expressed in the masu salmon brain during various periods of postembryonic development, but the patterns of immunolocalization of labeled cells during early development (yearling juveniles) and in later periods (2-year-old juveniles and older) differ significantly (Pushchina et al., 2012). Pax6 labeling at the border of brain neuromeres has enabled researchers to determine the structure of these neuromeres, since it selectively reveals different types of cells located in the periventricular proliferative zones, as well as the migrating cells in the initial stage of neuronal differentiation located in the deeper subventricular layers (Pushchina et al., 2013).

Previous studies conducted on adult trout showed the induction of proliferation and neurogenesis in the neurogenic niches in the brain integration centers, the optic tectum and cerebellum, after injury of the optic nerve in trout (Pushchina et al., 2016a). Proliferative activity was also detected in cells of the damaged optic nerve (Pushchina et al., 2016b).

The goal of this study was to investigate the distribution and localization of the $Zn8^{+}$ axon regeneration factor in the injured and contralateral optic nerves and the Pax6 transcription factor in various areas of adult trout brain (in which Pax6 was previously detected in salmonid fishes in the early postembryonic period of development) after a mechanical injury of the retina and optic nerve.

Materials and Methods

Animals

In this study, we used 90 adult male rainbow trout (*Oncorhynchus mykiss*), aged 12–18 months, with a body length of 40–46 cm and weighing 300–450 g, which were obtained from the Ryazanovka Fish Hatchery, Russia. The rainbow trout (*Oncorhynchus mykiss*) were kept at 16–17°C with a 14/10-hour light/dark cycle and fed once a day. The dissolved oxygen content of the water was 7–10 mg/dm^3, which corresponds to a normal level. All experimental manipulations with animals were carried out in accordance with the rules established by the National Scientific Center of Marine Biology (NSCMB), Far Eastern Branch Russian of the Russian Academy of Science (FEB RAS), and by the Commission on Biomedical Ethics of National Scientific Center of Marine Biology of the Far Eastern Branch of the Russian Academy of Sciences (approval No. 3) on February 25, 2018. Animals were anesthetized by placing in 0.1% solution of tricaine methanesulfonate MS222 (Sigma-Aldrich, St. Louis, MO, USA) for 10–15 minutes.

Tissue sample preparation for immunohistochemical (IHC) study

After anesthesia, 0.1 M phosphate buffer (pH 7.2) containing 4% paraformaldehyde solution was injected into the intracranial cavity of the immobilized animals. After prefixation, the brain was removed from the intracranial cavity and fixed in a paraformaldehyde solution at 4°C for 2 hours. The brain was then washed five times in a solution of 30% sucrose at 4°C for 48 hours for cryoprotection. Serial frontal and transversal sections of the brain were made on a freezing microtome Cryo-Star HM 560 MV (Carl Zeiss, Oberkochen, Germany).

Mechanical injury of the right eye of rainbow trout

The mechanical injury was inflicted according to methods previously described (Pushchina et al., 2016a, b). Using a sterile needle (Carl Zeiss, Oberkochen, Germany), a mechanical damaging impact was applied to the eye area to a depth of 1 cm, at which the cornea and mucous membrane of the eye, the retina, the lens, and the ONH with the adjacent tissues were damaged. The changes in the histological structure of adjacent oculomotor muscle fibers, the IHC labeling of proliferating cell nuclear antigen (PCNA) in the optic nerve cells, and the identification of cells with signs of apoptosis in the damaged optic nerve, indicating a change in its structure due to mechanical trauma, were discussed earlier (Pushchina et al., 2016a). As a result of traumatic effects, the central part of the retina, the pigment epithelium of the retina, the ONH with the adjacent oculomotor muscles (Pushchina et al., 2016b) were damaged. The contralateral optic nerve was used as a control. Immediately after inflicting the mechanical damage, the animals were released into a tank with fresh water for recovery and further monitoring.

IHC staining

An immunoperoxidase labeling of the optic nerve and brain was performed to investigate the localization of the Zn8 axon regeneration factor in the optic nerve and Pax6 transcription factor in the telencephalon, diencephalon, optic tectum, and brainstem after unilateral eye injury in rainbow trout (*Oncorhynchus mykiss*). Activity of Pax6 transcription factor and Zn8 axon regeneration factor was assessed at 1 week post-injury. IHC staining was performed to investigate the localization of Zn8 in growing axons and glial cells in optic nerves. Zn8 was identified using the standard streptavidin-biotin-peroxidase labeling on free-floating sections. The 50-μm-thick sections of the optic nerve were incubated *in situ* with anti-neurolin antibody (Zn8, monoclonal, mouse; Hybridoma Bank, Antibody Registry ID: AB_531904; CA, USA 1:300) at 4°C for 48 hours. For visualization of IHC labeling, a Vectastain Elite ABC kit (Vector Laboratories, Burlingame, CA, USA) was used. For identification of the reaction products, substrate of red color (VIP Substrate Kit,

Vector Labs, Burlingame, CA, USA) was used. The staining process was controlled under an Axiovert Apotome 200 inverted microscope (Carl Zeiss MicroImaging, Göttingen, Germany). The sections were rinsed with water, mounted on slides, dehydrated according to the standard protocol, and embedded in the BioOptica medium (ZytoVision GmbH, Milano, Italy).

Monoclonal antibodies against the Pax6 transcription factor (clone: AD2.38, Cat. No. MAB5522 Chemicon, Billerica, MA, USA, 1:400) were used to detect Pax6 transcription factor in frozen brain sections. To visualize the IHC labeling, the standard ABC complex Vectastain Elite ABC kit (Cat. No. 6100, Vector Laboratories, USA) was used in accordance with the manufacturer's recommendations. To identify the reaction products, a substratum of red color (VIP Substrate Kit, Vector Labs, Burlingame, CA, USA) was used in combination with methyl green staining. The brain sections were dehydrated using a standard technique and embedded in the BioOptica medium (Milano, Italy).

To assess the specificity of IHC reaction, the negative control method was used. Sections of the brain were incubated with 1% solution of non-immune horse serum, instead of primary antibodies, for 1 day and processed as sections with primary antibodies. In all the control experiments, no immunoreactivity was detected.

A densitometric study of IHC intensity of Zn8 and Pax6 labeling in optic nerve cells of the trout brain was performed using the Axiovision software supplied with the Axiovert Apotome 200 inverted microscope. Based on the densitometric analysis, various levels of Zn8 and Pax6 activity in cells were determined. These data, along with the morphometric parameters of cells and fibers, were used to classify and characterize immunoreactive cells, radial glia (RG), and non-glial precursors formed in the post-injury period.

Enzyme-linked immunosorbent assay (ELISA) immunoassay

After eye injury, the level of Pax6 in the brain of control animals was quantitatively determined using a commercial kit (MBS059499; Mir Biotech, San Diego, CA, USA). The ELISA analysis was conducted in tissues from 25 intact rainbow trout and 25 rainbow trout with unilateral eye injury (UEI). The brain of the rainbow trout was removed from the skull in 0.02 M phosphate buffer, weighed, and thoroughly washed in ice-cooled 0.02 M phosphate buffer (pH 7.2) to remove blood. Then the brain was mechanically cut into small pieces of 5 mL in the phosphate buffer in a Potter-Elvehjem polytetrafluoroathylene (PTFE) glass homogenizer (Sigma-Aldrich) on ice. The rainbow trout brain homogenates contained 10 mg tissue per 100 μL of PBS. The resulting suspension was processed in an ultrasonic homogenizer Sonoplus 2070 (Bandelin, Berlin, Germany) to destroy cell membranes. The homogenates were then centrifuged for 15 minutes at 1500 × *g* in a rotor (Beckman Coulter Ti50, Palo Alto, CA, USA). The supernatant was analyzed using a standard immunoperoxidase identification system, FishPad Bix Gene 6 ELISA Kit (MBS, San-Diego, CA, USA) according to the manufacturer protocol. A standard solution was used for standardization. The assay was carried out in a proprietary 96-well microtiter plate. The optical density was measured on a densitometer (Microelisa Stripplate Reader, Bio-Rad, Hercules, CA, USA) at a wavelength of 450 nm for 15 minutes.

Morphometric analysis

A morphometric analysis was performed using the software of an Axiovert 200 M inverted microscope equipped with an ApoTome module and Axio Cam MRM and Axio Cam HRC (Carl Zeiss, Germany) digital cameras. The measurements were performed at 400× magnification in five randomly chosen fields of view for each area examined.

Statistical analysis

The morphometric data of IHC labeling of Zn8 and Pax6 were quantitatively processed using STATA statistical software (StataCorp. 2012. Stata Statistical Software: Release 12. College Station, TX: StataCorp LP, USA) and Microsoft Excel 2010 (Microsoft Office Professional E435-2642, Moscow, Russian Federation). All data are expressed as the mean ± SD and analyzed with the SPSS software (version 16.0; SPSS, Chicago, IL, USA). All variables measured in groups were compared using Student's *t*-test or one-way analysis of variance (ANOVA) followed by the Student-Newman-Keuls *post hoc* test. Values at $P < 0.05$ were considered statistically significant.

Results

Neurolin immunoreactivity in rainbow trout optic nerves

Immunolocalization of Zn8 was detected in a heterogeneous population of glial cells and nuclei on the ipsilateral (damaged) side, as well as in individual $Zn8^+$ optic nerve fibers on the contralateral side. The morphological parameters of $Zn8^+$ cells are provided in **Table 1**.

Single small $Zn8^+$ astrocytes and rare aggregates of small $Zn8^+$ cells were detected in the contralateral nerve after UEI (**Figure 1A**). In the medial optic nerve zone, $Zn8^-$ astrocytes and astroblasts exhibited similar migration patterns (**Figure 1A**). The density of distribution of $Zn8^+$ elements was low in the ONH: no more than 5–6 cells per visual field were counted on the contralateral side (**Figure 1B**). In the area of the chiasma optica, $Zn8^+$ regenerating axons and cells were observed near the contralateral nerve (**Figure 1C**). The morphological parameters of $Zn8^+$ cells indicate that they represent a population of astrocytes and astroblasts. Aggregates of germinating $Zn8^+$ axons were detected in the intraorbital segment (IOS) of the contralateral nerve (**Figure 1D**). A large aggregate of immunoreactive cells was identified in the proximal part of the optic nerve, and $Zn8^+$ cells located along the optic nerve were also detected, possibly representing crossed fibers (**Figure 1E**). Separate bundles of Zn8-labeled fibers and $Zn8^+$ astrocytes were observed in the distal part of the optic nerve, and elongated $Zn8^-$ migrating cells were observed in the central part of the optic nerve (**Figure 1F**).

The percentages of $Zn8^+$ and methyl green-stained cells in the contralateral nerve are shown in **Figure 2A**. The greatest percentage of $Zn8^+$ cells was detected in the proximal part of the optic nerve. Significantly greater numbers of $Zn8^+$ nuclei and cells were detected in the damaged nerve than on the contralateral side (**Figure 2B**). The maximum percentage

Table 1 Morphometric parameters of Zn8$^+$ and Zn8$^-$ cells in the optic nerve of rainbow trout, *Oncorhynchus mykiss*, at 1 week after unilateral eye injury

	Small cells (size of cells, μm)	Medium cells (size of cells, μm)	Large cells (size of cells, μm)	Nuclei of cells (size of nuclei, μm)
Zn8$^+$ ipsilateral	5.9±0.5/3.9±0.9	9.7±0.8/4.1±0.4	11.2±0.7/2.7±0.4	4.1±0.5/3.0±0.4
Zn8$^+$ contralateral	7.3±0.7/3.6±0.2	–	–	4.0±0.7/2.8±0.5
Zn8$^-$	8.4±0.9/4.5±1.2	–	12.5±1.2/3.7±0.5	6.2±0.5/4.1±0.7

Data are expressed as the mean ± SD.

of Zn8$^+$ nuclei was detected in the ONH, cells of the IOS, and the proximal part of the optic nerve (**Figure 2B**). The maximum number of Zn8$^+$ astrocytes was observed in the proximal part of the ipsilateral nerve, whereas the ONH and the distal part of the damaged nerve exhibited a lower percentage of Zn8$^+$ cells (**Figure 2C**). The percentages of Zn8$^+$ and Zn8$^-$ astrocytes in contralateral and ipsilateral nerves are shown in **Figure 2D**.

Significantly greater numbers of Zn8$^+$ cells and germinating axons were observed in the damaged optic nerve than in the contralateral nerve (**Figure 3A**). Zn8$^+$ cells formed dense clusters along the optic nerve fibers; the Zn8 axon regeneration factor was also often observed in regenerating fibers of the damaged nerve (**Figure 3A**). The quantitative analysis of immunoreactive elements in the injured nerve indicates the presence of a large number of Zn8$^+$ astrocyte nuclei with a high density of distribution (**Figures 2B** and **3A**). The maximum number of Zn8$^+$ nuclei and cells were detected in the ONH of the damaged nerve (**Figure 3B** and **D**). The IOS contained many fewer Zn8-immunoreactive nuclei, but increased numbers of Zn8$^+$ astrocytes and migrating cells were observed (**Figures 2B, 3C** and **3D**). Large numbers of Zn8$^+$ astrocytes of different morphologies and sizes and Zn8$^+$ nuclei were detected in the proximal part of the optic nerve (**Figure 3D** and **E**). Large numbers of Zn8$^-$ astrocytes and astroblasts were also present in the proximal part of the damaged nerve (**Figure 3E**). A heterogeneous population of Zn8$^+$ cells, nuclei, and immunoreactive axons was observed in the distal part (**Figure 3D** and **F**). Fewer Zn8$^+$ cells were observed in the distal part than in the proximal part (**Figure 3D**).

Pax6 concentrations in rainbow trout brain

According to the enzyme immunoassay (**Figure 4**), the concentration of Pax6 in the brain of intact rainbow trout in the control and UEI groups was 6.24 ± 0.03 pg/mL and 9.8 ± 0.11 pg/mL after UEI ($P < 0.001$). Thus, within a week after UEI, the concentration of the protein product of the Pax6 transcription factor was increased by approximately one third compared with control animals.

Pax6 immunoreactivity in rainbow trout brain

Telencephalon

The data from the densitometry analysis of the control animals showed two types of Pax6-immunolabeled cells that were present in the telencephalon: intensely and moderately labeled cells (**Figure 5A–E** and **Additional Table 1**). Intense Pax6 labeling (130 ± 9.7 units of optical density UOD) was detected in all morphological cell types (**Additional Table 1**). These cells were detected in three main regions of the dorsal area (dorsal [Dd], lateral [Dl], and central [Dc] parts of dorsal area; **Figure 5A–C**) and two regions of the ventral area (dorsal [Vd] and lateral [Vl] parts of ventral area; **Figure 5D** and **E**) of the telencephalon. Moderate Pax6 labeling (70 ± 12.6 UOD) was detected in cells of various types, representing a major proportion of labeled neurons in all areas of the telencephalon (**Figure 5A–E** and **Additional Table 1**). In most cases, the distribution of intensely labeled neurons was similar; single or paired cells were usually surrounded by more numerous moderately labeled neurons, forming clusters of different densities (**Figure 5A, C**, and **E**). The quantitative relationship between intensely and moderately labeled Pax6$^+$ cells is shown in **Figure 5F**.

After UEI, reactive neurogenic niches were observed in the periventricular zone of Dd that contained intensely labeled subventricular cells located under a layer of Pax6$^-$ cells (**Figure 6A** and **Additional Table 1**). The surface-located neuroepithelial Pax6$^+$ cells were small and undifferentiated, with a moderate level of Pax6 immunolabeling (**Figure 6A**). No Pax6$^+$ cells were detected in the deep layers of Dd (**Figure 6A**).

After UEI, Pax6$^+$ RG were detected in the dorsal and ventral areas of the telencephalon (**Figure 6B–F**). A dense network of RG fibers was identified in Dl; but it gradually decreased in the ventral direction (**Figure 6B**). The dimensions of RG were 11.3 ± 3/5.7 ± 1.3 μm; the optical density of RG labeling in the dorsal area was 134.2 ± 7.4 UOD. In the ventral area, the highest density of RG was observed in the lateral (Vl; **Figure 6C**) and ventral (Vv, parts of ventral zone; **Figure 6D**) zones. The morphological parameters of RG located in the ventral area are provided in **Additional Table 1**. More numerous aggregates of periventricular Pax6$^+$ cells were observed in Vl than in other regions, and the distribution of RG fibers was heterogeneous. In Vl, small but intensely Pax6-labeled reactive niches were observed in the subventricular layer, where radially oriented RG fibers were located (**Figure 6C**). Separate intensely and moderately Pax6-labeled oval-shaped cells were located in deeper layers of Vl (**Additional Table 1**). Small, intensely labeled neuroepithelial cells exhibited a surface localization (**Figure 6C**). The optical density of RG labeling was 136.7 ± 5.4 UOD.

The distribution of RG fibers in Vv was different from the distribution in Vl (**Figure 6D**). The fibers in Vv were organized as a discrete focus surrounded by vessels and immunonegative cells (**Figure 6D**). A similar structure of reactive neurogenic niches, including a heterogeneous population of cells surrounded by branched vessels, was observed in most areas of the telencephalon. A dense network of Pax6$^+$ fibers was observed in the surface layers of the periventricular zone; the Pax6$^+$ cells were arranged as local clusters in the subven-

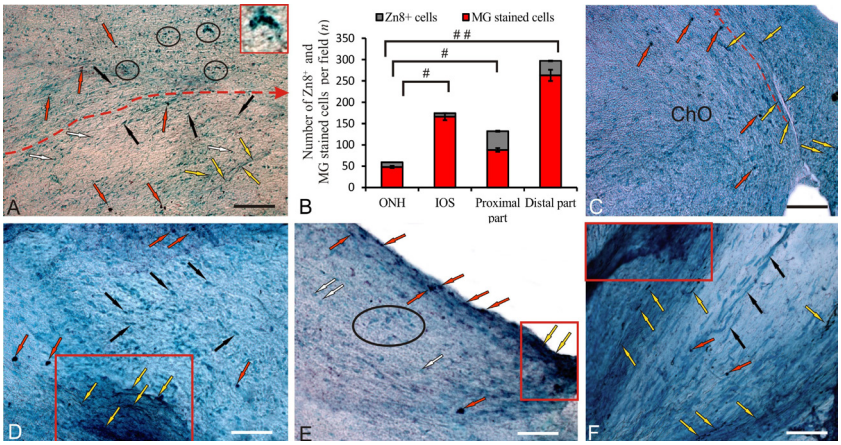

Figure 1 Localization of neurolin (a regeneration-associated, Zn-8 labeled protein) in the contralateral optic nerve of rainbow trout, *Oncorhynchus mykiss*, at 1 week after unilateral eye injury (UEI).

(A) Immunolabeling of Zn8 in the middle part of the contralateral nerve: $Zn8^+$ cells (indicated by red arrows), $Zn8^-$ rounded cells (white arrows), $Zn8^-$ elongated cells (black arrows), $Zn8^+$ axons (yellow arrows), and $Zn8^+$ cells and clasters (inset) in the central part of the optic nerve (outlined by ovals); the red dotted line delimits the middle portion of the nerve and shows the direction of cell migration. (B) Ratio of $Zn8^+$ and methyl green (MG) stained cells (mean ± SD) in the optic nerve head (ONH), intraorbital segment (IOS), proximal and distal parts of the contralateral nerve (n = 5 in each group; #P < 0.05, ##P < 0.01; one-way analysis of variance (ANOVA) followed by the Student-Newman-Keuls *post hoc* test); the error bars correspond to the standard deviation. (C) Immunolabeling of Zn8 in the optic chiasma (arrow indications here and below see in A). (D) Immunolabeling of Zn8 in the IOS with an aggregation of germinating $Zn8^+$ axons (in red rectangle). (E) Immunolabeling of Zn8 in the proximal part of the contralateral nerve with an aggregation of germinating axons (in the red rectangle) and aggregation of $Zn8^-$ astrocytes (in black oval). (F) Immunolabeling of Zn8 in the distal part of the contralateral nerve; degenerating $Zn8^-$ fibers are indicated by black arrows (other arrow indications see above). Peroxidase $Zn8^-$ immunolabeling on optic nerve sections with methyl green staining. Scale bars: A, 100 μm; C–F, 50 μm.

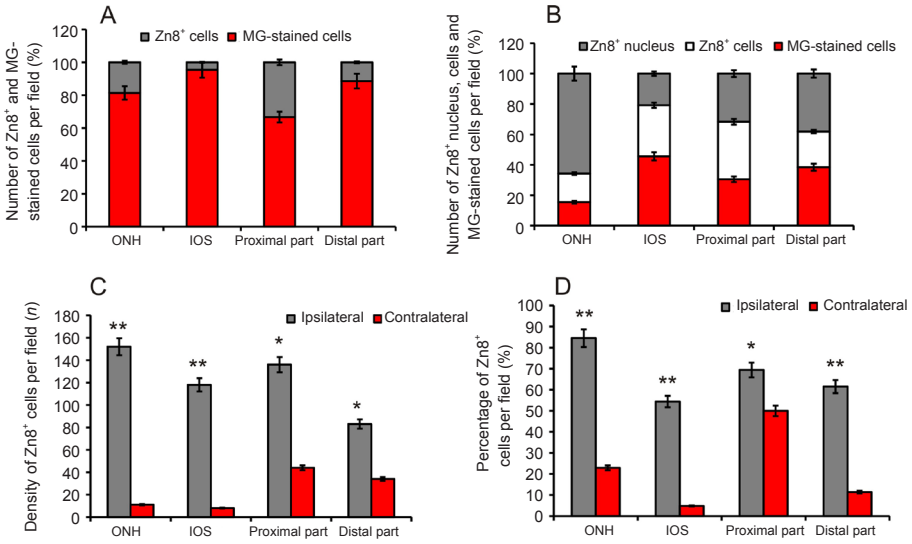

Figure 2 $Zn8^+$ and $Zn8^-$ cells density in the optic nerves of rainbow trout, *Oncorhynchus mykiss*, at 1 week after unilateral eye injury.

(A) Percentage of $Zn8^+$ and methyl green (MG)-stained cells in the optic nerve head (ONH), intraorbital segment (IOS), and the proximal and distal parts of contralateral nerve (mean ± SD). (B) Percentage of $Zn8^+$ nucleus, $Zn8^+$ cells, and methyl green (MG)-stained cells on the side of damage (mean ± SD). (C) Density of $Zn8^+$ cells in contralateral and ipsilateral optic nerves per 400-fold visual field, one-way analysis of variance (ANOVA) followed by the Student-Newman-Keuls *post hoc* test was used to determine significant differences in contralateral and ipsilateral nerves (n = 5 in each group; *P < 0.05, **P < 0.01, *vs.* contralateral nerves). (D) Percentage of $Zn8^+$ astrocytes in the contralateral and ipsilateral nerves (n = 5 in each group; *P < 0.05, **P < 0.01, *vs.* contralateral nerves).

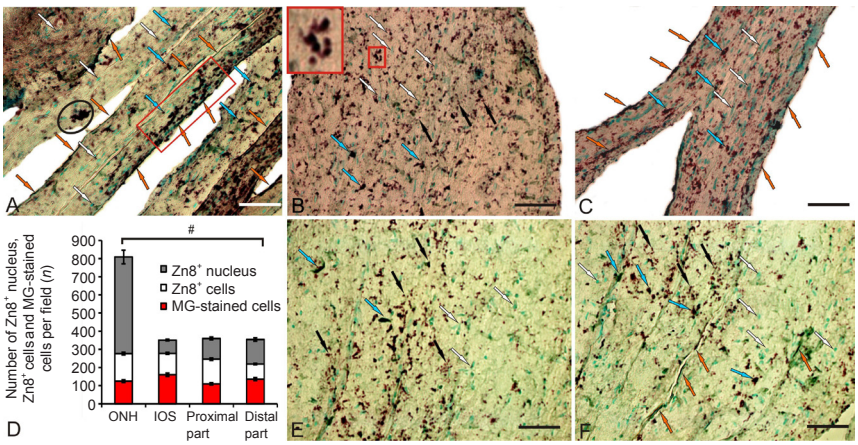

Figure 3 Localization of neurolin in the damaged optic nerve of trout, *Oncorhynchus mykiss*, at 1 week after unilateral eye injury.

(A) Immunolabeling of Zn8 in the middle part of the nerve: $Zn8^+$ astrocytes (blue arrows), $Zn8^-$ astrocytes (white arrows), $Zn8^+$ axons (orange arrows), a small cluster of $Zn8^+$ cells in the central part of the nerve (encircled by black oval), and a cluster of $Zn8^+$ migrating cells and fibers (in red rectangle). (B) Immunolabeling of Zn8 in the optic nerve head (ONH); a small cluster of $Zn8^+$ cells (inset), subcellular $Zn8^+$ inclusions are indicated by black arrows. (C) Immunolabeling of Zn8 in the intraorbital segment (IOS); MG-stained migrating astrocytes are indicated by white arrows. (D) Number of $Zn8^+$ nucleus, $Zn8^+$ cells, and methyl green (MG)-stained cells (mean ± SD) in the ONH, IOS, and the proximal and distal parts per visual field in the damaged nerve (n = 5 in each group, #P < 0.05; one-way analysis of variance (ANOVA) followed by the Student-Newman-Keuls *post hoc* test). (E) Immunolabeling of Zn8 in the proximal part of the damaged nerve. (F) Immunolabeling of Zn8 in the distal part of the damaged nerve (see other designations above). Peroxidase Zn8-immunolabeling in optic nerve sections with methyl green staining. Scale bars: 50 μm for A–C, E, and F.

tricular zone. Individual intensely and moderately labeled Pax6$^+$ cells were detected in deep telencephalic layers (**Figure 6D** and **Additional Table 1**). In Vd, the RG were organized as small beams separated by gaps (**Figure 6E** and **Additional Table 1**). The somas of Pax6$^+$ cells were located in the subventricular layer; small labeled elements forming a sparse network were observed in the periventricular layer (**Figure 6E**). A significantly higher density of Pax6$^+$ fibers and RG was observed in the ventral area ($P < 0.05$) than in the dorsal area (**Figure 6F**).

Diencephalon

In the diencephalon of the control animals, the Pax6 immunoreactivity was detected in the magnocellular (POm; **Figure 7A**) and parvocellular (Pop; **Figure 7B**) nuclei of the preoptic area, the periventricular nuclei of the dorsal (Dth; **Figure 7C**), medial (Mth; **Figure 7D**), and ventral thalamus (Vth; **Figure 7E**), and in the anterior thalamic nucleus (Ath; **Figure 7F**). The morphological and densitometric parameters of Pax6$^+$ cells in the nuclei of diencephalon in the control animals are presented in **Additional Table 1**.

In the dorsal parvocellular part of the preoptic area, numerous undifferentiated Pax6$^+$ cells were found in the periventricular and subventricular areas after UEI (**Figure 8A** and **B**). Reactive niches containing intensely labeled Pax6$^+$ cells were detected in the periventricular and subventricular zones, and parenchymal layers of POp (**Figure 8B**). A greater number of reactive niches were observed in the POp than in the POm. Medium-sized and small oval-shaped cells with a high intensity of Pax6 labeling were often identified in the POp (**Figure 8B** and **Additional Table 1**). The migrating cells were located in the deeper layers of the dien-

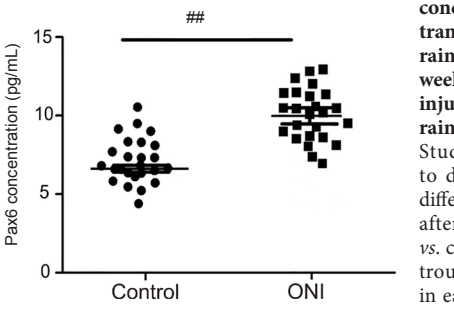

Figure 4 ELISA assay of concentrations of Pax6 transcription factor in the rainbow trout brain at 1 week after unilateral eye injury *vs.* control (intact) rainbow trout.
Student's *t*-test was used to determine significant differences between 1 week after unilateral eye injury *vs.* control (intact) rainbow trout (##$P < 0.01$), $n = 25$ in each group. ONI: Optic nerve injury.

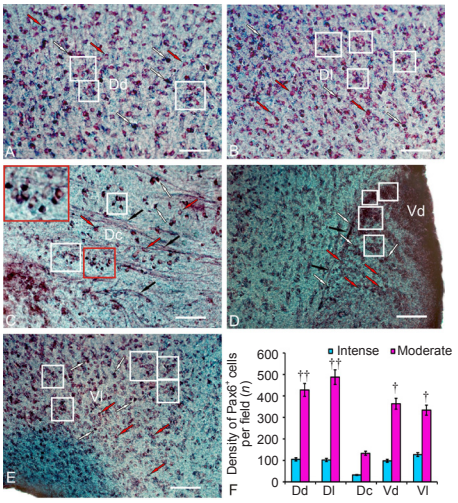

Figure 5 Localization of Pax6 transcriptional factor in the telencephalon of an intact rainbow trout, *Oncorhynchus mykiss*.

(A) In the dorsal zone of the dorsal area (Dd): intensely labeled cells are indicated by white arrows; moderately labeled cells are indicated by red arrows; and clusters of moderately labeled cells are outlined by white squares. (B) Lateral zones of the dorsal area (Dl). (C) In the central part of the dorsal area (Dc): labeled fibers are indicated by black arrows; heterogeneously labeled clusters of immunoreactive cells in white squares (inset shows a cluster at higher magnification). (D) Dorsal nucleus of the ventral area (Vd). (E) Lateral part of the ventral area (Vl). Immunoperoxidase labeling of Pax6 and staining with methyl green on transversal brain sections. Scale bars: 100 μm for A–E. (F) Ratio of intensely and moderately Pax6-labeled cells (mean ± SD) in the dorsal (Dd), lateral (Dl), central (Dc) zones of the dorsal area and in the dorsal (Vd) and lateral (Vl) zones of the ventral area of telencephalon in intact rainbow trout per 200-fold visual field, one-way analysis of variance (ANOVA) followed by the Student-Newman-Keuls *post hoc* test was used to determine significant difference between the number of moderately and intensely labeled cells ($n = 5$ in each group, †$P < 0.5$, ††$P < 0.01$, *vs.* intensely labeled cells).

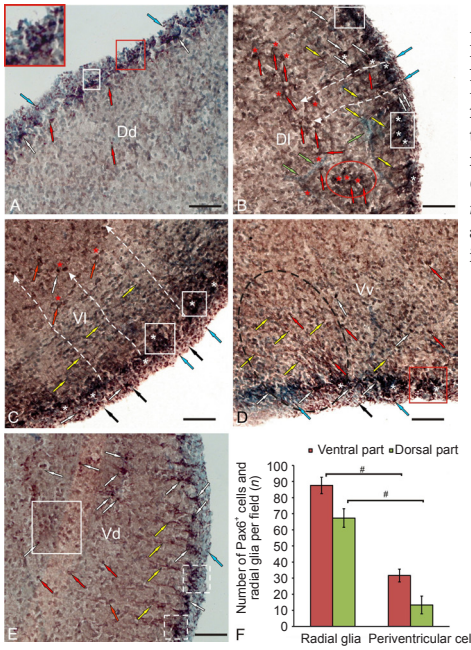

Figure 6 Localization of the Pax6 transcription factor in the telencephalon of rainbow trout, *Oncorhynchus mykiss*, at 1 week after unilateral eye injury.

(A) In the dorsal zone of the dorsal area (Dd), intensively labeled subventricular cells are indicated by white arrows; moderately labeled subventricular cells are indicated by red arrows; neuroepithelial cells are indicated by blue arrows; reactive neurogenic niches are outlined by white squares, in inset reactive neurogenic niches at higher magnification. (B) In the lateral zone of the dorsal area (Dl): fibers of radial glia are indicated by yellow arrows; endothelial cells of vessels are indicated by green arrows; moderately labeled cells migrating along the radial glia fibers are in the red oval; Pax6$^-$ cells in the reactive parenchymal niches are indicated by red asterisks; Pax6$^-$ cells in neuroepithelial reactive niches are indicated by white asterisks; white dashed lines show the directions of radial cell migration; see other designations in A. (C) In the lateral zone of the ventral area (Vl), Pax6$^-$ neuroepithelial cells are indicated by black arrows; see other designations in A and B. (D) In the ventral nucleus of the ventral area (Vv), an aggregation of radial glia fibers is outlined by black dashed oval; a reactive niche is indicated by red square. (E) In the dorsal nucleus of the ventral area (Vd), reactive neurogenic niches are outlined by white dashed squares; a cluster of moderately labeled parenchymal cells are indicated by a large white square. Immunoperoxidase labeling of Pax6 and staining with methyl green on transversal brain sections. Scale bars: 100 μm for A–E. (F) Number of intensely Pax6-labeled undifferentiated cells and radial glia (mean ± SD) in the dorsal and ventral areas of the telencephalon in the rainbow trout after unilateral eye injury per 200-fold visual field, one-way analysis of variance (ANOVA) followed by the Student-Newman-Keuls *post hoc* test was used to determine significant difference between the number of radial glia and periventricalar cells in ventral and dorsal parts ($n = 5$ in each group, #$P < 0.05$).

cephalon (**Figure 8A** and **Additional Table 1**). After injury, a network of Pax6$^+$ RG was detected in the ventral magnocellular part of the preoptic area (**Figures 8A, 8C** and **9B**), as well as in undifferentiated and oval cells in the periventricular and subventricular areas (**Figure 8C**). Numerous reactive niches with intensely labeled Pax6$^+$ cells were observed in the periventricular area (**Figure 8C**). Rare niches displaying a heterogeneous cell composition with moderate Pax6 activity were identified in the subventricular zone of POm (**Figure 8C**). Single niches with a parenchymal localization containing rare, small Pax6$^+$ cells were observed in deep diencephalic layers (**Figure 8C**). The morphometric and densitometric parameters of periventricular and subventricular POm cells are shown in **Additional Table 1**. A matrix zone corresponding to the borders of the P2/P3 neuromeres was identified in the dorsal thalamus (**Figure 8D**). A dense network of RG fibers was detected in the region of the dorsal P2 and ventral P3 neuromeres (**Figure 8D** and **E**). Numerous reactive niches located in the periventricular, subventricular, and parenchymal diencephalic regions (**Figure 8D**) were identified in the area of the dorsal P2 neuromere (in the Dth region). The reactive niches were predominantly located in the periventricular layer (**Figure 8E**). The cellular composition of the periventricular and subventricular areas of Dth, Mth, and Vth was morphologically heterogeneous (**Additional Table 1**). Very high intensity Pax6 labeling was observed in small, undifferentiated and oval cells in the periventricular region of the thalamus (**Additional Table 1**). High and moderate intensity Pax6 labeling was recorded in the migrating cells in the subventricular zone and deep diencephalic layers (**Additional Table 1**). A dense cluster of Pax6 cells was identified at the border of P2 and P3 neuromeres after injury (**Figure 8D**), but it was not detected in intact animals (**Figure 7C** and **D**).

In the posterior tuberal nucleus, a large number of RG fibers were observed around the fasciculus retroflexus (fr; **Figure 8F**) and in the ventral thalamic area (**Figure 8I** and **J**). Dense aggregates of Pax6$^+$ cells were detected in the dorsal and ventral periventricular zones of the PTN (**Figure 8F**). We postulate that the same reactive niches occur at the borders of the ventral prosencephalic neuromeres (P3–P5) after UEI. In the posterior tuberal nucleus, clusters of Pax6$^-$ cells, which were similar to the clusters in the dorsal thalamus at the P2 and P3 borders (**Figure 8F** and **J**), were observed at the border of P3 and P4 neuromeres.

High intensity Pax6 labeling was detected in the anterior thalamic nucleus (Ath) after optic nerve injury (**Additional Table 1**). Reactive clusters of small undifferentiated Pax6$^+$ cells were observed in the central part of the Ath. Heterogeneous reactive niches containing Pax6-labeled cells were also detected around the Ath and on the periphery of the Ath after UEI (**Figure 8G** and **Additional Table 1**) but were absent in intact animals (**Figure 7F**). Reactive niches and single undifferentiated Pax6$^+$ cells were present in the periglomerular area (**Figure 8G**). In the medial thalamus (Mth), a Pax6$^+$ cell cluster was detected in the subventricular region. Pax6$^-$ undifferentiated cells were predominantly located in the periventricular zone and in deeper layers of the Mth (**Figure 8H**). Numerous reactive niches and RG fibers were identified in the periventricular zone of the ventral thalamus (Vth) (**Figure 8I**). Heterogeneous reactive niches with a highly dense cell distribution containing moderately labeled Pax6$^+$ cells were observed in the subventricular zone of the Vth (**Figure 8I**). In the parenchymal zone of Vth, Pax6$^-$ neurogenic niches were identified after UEI (**Figure 8I**), but not in the control animals (**Figure 7E**). Most cells of the periventricular region of the PTN exhibited a similar size and shape to cells located in the preoptic area. An aggregate of Pax6$^+$ cells in the periventricular area of the dorsal PTN was located at the border of neuromeres (**Figure 8H** and **J**).

In the rainbow trout diencephalon, we observed a significant increase in the number of neuroepithelial cells contacting the ventricular lumen (**Figure 8K**). A large number of Pax6$^+$ cells were observed in the subventricular zone, and numerous migrating cells were present in the MZ of the diencephalon (**Figure 8K**). In **Figure 8K**, the dashed lines indicate the migration of cells from the periventricular region of the Dth to the deep layers of the diencephalon toward the Ath. After the traumatic injury, the Pax6-labeled RG fibers were also traced in the Vth from the periventricular region surrounding the P4 and P5 neuromeres to the deep layers of the diencephalon (**Figure 8F**, **I**, and **J**), but more intense labeling of RG fibers was observed near the P2 and P3 neuromeres. In the region of the pretectal (P1) neuromere (**Figure 8L**), the Pax6$^+$ cells formed a dense morphogenetic field in the area adjacent to fasciculus retroflexus after UEI (**Figure 8L**).

The data obtained from the quantitative analysis revealed an increase in the number of Pax6$^+$ cells and RG in the periventricular diencephalon and in the adjacent regions containing migrating cells after UEI (**Figure 9A–D**). In the POp, we observed a highly significant increase in the number of intensely labeled Pax6$^+$ neurons ($P < 0.01$) and a significant increase in the number of moderately labeled Pax6$^+$ cells ($P < 0.05$) (**Figure 9A**). In the POm, significant increases in the numbers of intensely and moderately labeled Pax6$^+$ cells, as well as Pax6$^-$ cells stained with methyl green ($P < 0.05$), were observed (**Figure 9B**). In the Dth, a highly significant increase in the number of intensely labeled Pax6$^+$ cells ($P < 0.01$) and significant increases in the numbers of moderately labeled Pax6$^+$ cells and Pax6$^-$ cells stained with methyl green ($P < 0.05$) were observed (**Figure 9C**). In the Vth, a highly significant increase in the number of intensely labeled Pax6$^+$ neurons ($P < 0.01$) and a significant increase in the number of Pax6$^+$ cells stained with methyl green ($P < 0.05$) were identified (**Figure 9D**).

Optic tectum

In the tectum of the control animals, Pax6 labeling was located in the stratum marginale (SM), stratum griseum centrale (SGC), stratum griseum et album superficiale (SGAS), stratum album centrale (SAC) and stratum griseum periventriculare (SGP) (**Figure 10A**). Two types of cells were identified in the SM and SGP: undifferentiated small and oval cells (**Figure 10** and **Additional Table 1**). Bipolar cells of various sizes and morphologies were identified in the deep layers of the tectum (SGC, SGAS and SAC) (**Figure 10B** and **Additional Table 1**).

After UEI, intensely labeled Pax6$^+$ RG cells were detected

in the SM of the tectum. Unlike intact animals, animals subjected to UEI did not display intense Pax6 immunolabeling in neurons of all tectal layers; however, a large number of single, small, undifferentiated Pax6$^+$ cells and small clusters of these cells located in reactive niches were identified in all topographic zones of the tectum (**Figure 10C** and **D**).

In the dorsal zone of the tectum, few RG were observed (**Figure 11A**). RG were morphologically heterogeneous and displayed high intensity of Pax6 immunolabeling (**Figure 10C, D** and **Additional Table 1**). A layer of Pax6$^-$ small cells was observed above the highly immunoreactive RG layer. The latter formed neuroepithelial reactive niches, the cells of which were stained with methyl green (**Figure 10C** and **D**). Small, rounded, single intensely labeled Pax6$^+$ cells or cells forming small clusters comprised the reactive niches (**Figure 10D**). Pax6$^-$ local cell clusters were observed in the layer of optical fibers (**Figure 10C**). Radially migrating Pax6$^+$ cells were sometimes observed along the RG fibers (**Figure 10C** and **E**). The highest concentrations of migrating Pax6$^+$ cells were located in the SGC and in deeper sites of the SAC (**Figure 10E** and **F**).

In the medial zone of the tectum, a higher density of RG was observed in the marginal layer than in the dorsal zone (**Figure 10D** and **F**). The number of intensely labeled RG in the medial zone also exceeded the number detected in the dorsal zone (**Figure 11A**). Above the layer of RG, single conglomerates of intensely labeled Pax6$^+$ cells without radial outgrowths were observed above the layer of RG (**Figure 10E** and **F**). In contrast to the dorsal zone, the Pax6$^+$ cells of the medial zone in the SM were stained with methyl green, but did not form clusters (**Figure 10E** and **F**). The dense populations of Pax6$^+$ cells migrating along the RG fibers in SGC and SGAS were similar to those in the dorsal zone (**Figure 10C** and **E**). In the SGP, moderate Pax6 immunolabeling was observed in some cells and radial fibers running along the large reactive niches formed by immunonegative cells of the periventricular layer (**Figure 10E**). A low level of Pax6 immunolabeling was observed in the deep tectal layers of the medial zone. Only single, small, intensely labeled Pax6$^+$ cells and moderately labeled, large, bipolar cells were detected (**Figure 10E** and **Additional Table 1**).

The maximal density of RG was recorded in the SM and high intensity Pax6 labeling in the RG was observed in the lateral zone of the OT (**Figures 10G**, **10H**, and **11A**). The OT was significantly thicker in the caudal region than in the rostral and central regions, particularly in the lateral zone, where the SGP exhibited significant hypertrophy (**Figure 10G**). In the lateral zone, several Pax6$^+$ RG were organized into small bundles comprising 2–3 units, whose processes extended a considerable distance from the SM to the layer of optic fibers (**Figure 10H**). Large reactive niches comprising small, undifferentiated, weakly labeled Pax6$^+$ or Pax6$^-$ cells were identified. These cells were migrating along RG fibers in the SGC and SGAS (**Figure 10G**). Aggregates of moderately labeled Pax6$^+$ cells were detected in the lateral optic tract and in the deeper layers of the caudal proliferative zone of the SGP (**Figure 10G**). Moderate or high intensity Pax6 labeling was observed in cells of the SGP (**Additional Table 1**). The sites containing Pax6$^+$ cells in SGP were supplemented by numerous groups of Pax6$^-$ cells, which were stained with methyl green (**Figure 10G**). Similar to the dorsal and medial tectal zones, the local reactive niches containing small, intensely labeled Pax6$^+$ cells were located above the layer of intensely labeled RG cells in the lateral zone. These labeled cells lacked processes adjacent to dense Pax6$^-$ clusters of cells stained with methyl green (**Figure 10H**). We also refer to these dense cellular aggregates as reactive neurogenic niches, which were particularly common in the caudal proliferative zone of the tectum. In contrast to the dorsal and medial zones of tectum, the neurogenic niches in the lateral zone were more numerous and larger after UEI (**Figure 10H**).

The results of the analysis of quantitative distribution of Pax6$^-$labeled cells and RG in the tectum of intact rainbow trout and rainbow trout with UEI are shown in **Figure 11**. A comparative analysis of the distribution of Pax6$^+$ RG in the dorsal, medial, and lateral zones of the SM showed a corresponding increase in the number of RG in all zones, but significant differences between the zones were not observed (**Figure 11A**). The comparative distribution of Pax6$^+$ RG in SM was substantially ($P < 0.01$) increased after UEI (**Figure 11B**). An essential increase in the number of Pax6$^-$ cells ($P < 0.05$) stained with methyl green was also observed after injury, while the number of moderately labeled Pax6$^+$ cells increased insignificantly (**Figure 11B**). A few intensely labeled Pax6$^+$ neurons were detected in the SGC of control animals (**Figure 11C**). After UEI, no intensely labeled Pax6$^+$ cells were detected, but a substantial increase in the number of moderately labeled cells ($P < 0.05$) and a slight decrease in the number of Pax6$^-$ cells were recorded compared to the control (**Figure 11C**). In SGAS of the intact rainbow trout, we also identified various types of intensely labeled Pax6$^+$ neurons that were not detected after UEI (**Figure 11C** and **D**). After UEI, the number of moderately labeled cells in the SGAS ($P < 0.01$) and the number of Pax6$^-$ cells ($P < 0.05$) stained with methyl green increased significantly (Figure 11D). In the SAC, the number of Pax6$^+$ cells was not significantly increased, but the number of Pax6$^+$ cells was essentially less than ($P < 0.01$) the number observed in the control animals (**Figure 11E**). In the SGP, an increase ($P < 0.01$) in the number of moderately labeled Pax6$^+$ cells was revealed after UEI (**Figure 11F**).

Brainstem

Intense Pax6 labeling was detected in the periventricular region, cells adjacent to the pial membrane, projection neurons of the reticular formation, and nuclei of cranial nerves in the brainstem of the control animals (**Figure 12A** and **B**, and **Additional Table 1**). Intense Pax6 labeling was detected in several types of neurons (**Additional Table 1**) and in periventricular cells of the dorsal tegmental nuclei. A high level of Pax6 immunoreactivity was detected in the areas of primary proliferation, nuclei of cranial nerves, and neurons of the reticular formation (**Figure 12A** and **B**, and **Additional Table 1**).

In the tegmentum, superficially located conglomerates of undifferentiated ependymoglial Pax6$^-$ cells were detected after UEI. These cells formed local clusters at the borders of mesencephalic neuromeres (**Figure 12C**). Reactive niches

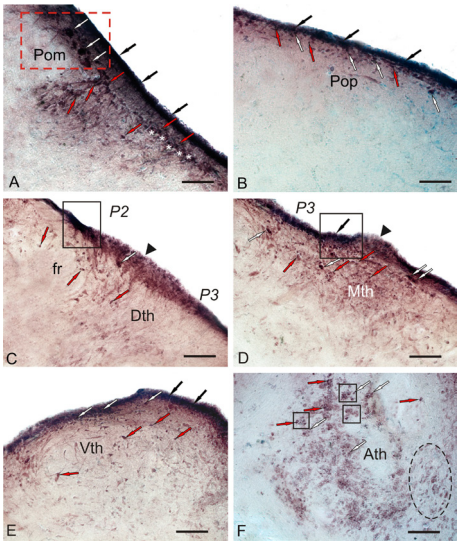

Figure 7 Localization of Pax6 in the diencephalon of intact rainbow trout, *Oncorhynchus mykiss*.

(A) In the magnocellular preoptic nucleus (POm) (outlined by red dotted line); large Pax6$^+$ neurons are indicated by white arrows; small Pax6$^+$ neurons are indicated by red arrows; Pax6$^+$ periventricular cells are indicated by black arrows; Pax6$^-$ cells are indicated by white asterisks. (B) Parvocellular preoptic nucleus (POp). (C) In the dorsal thalamic nucleus (DTh), a cluster of intensely Pax6-labeled undifferentiated cells are indicated by a white arrow; moderately Pax6-labeled cells surrounding fasciculus retroflexus (fr) are indicated by red arrows; neuroepithelial constitutive neurogenic niche (black arrowhead) surrounding the intensely labeled periventricular clusters of Pax6$^+$ cells (in black rectangle) corresponds to P2 and P3 neuromeres. (D) Medial thalamus (Mth). (E) Ventral thalamic nucleus (Vth). (F) In the anterior thalamic nucleus (Ath), constitutive neurogenic niches are outlined by black squares; aggregation of weakly labeled cells is indicated by a black dashed oval. Immunoperoxidase labeling of Pax6 and staining with methyl green on transversal brain sections. Scale bars: 100 μm.

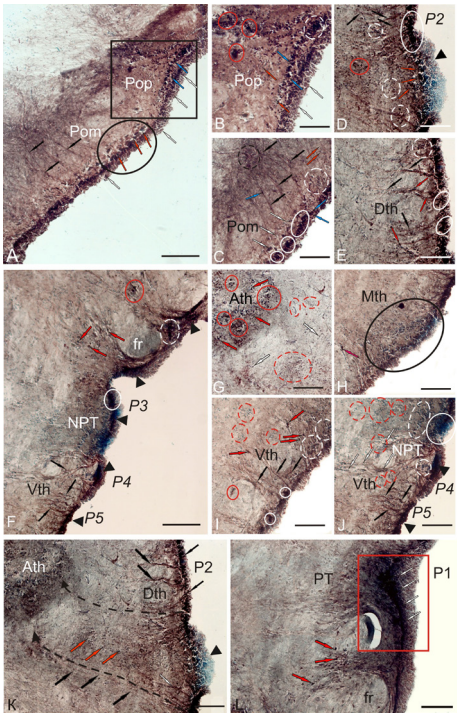

Figure 8 Localization of Pax6 in the diencephalon of rainbow trout, *Oncorhynchus mykiss*, at 1 week after unilateral eye injury.

(A) General view of parvocellular preoptic nucleus (POp; in square) and magnocellular preoptic nucleus (POm; in oval), fibers of radial glia (black arrows), subventricular reactive niches (blue arrows), Pax6$^-$ neuroepithelial cells (white arrows), and Pax6$^-$ neurosecretory cells (red arrows). (B) In the POp, Pax6$^-$ cells of deep layers (red arrows), a subventricular reactive niche (white dotted line), and reactive niches of parenchymal localization (in red ovals) are observed. (C) In the rostral part of POm, neuroepithelial reactive niches are outlined by white ovals; the segment of convergence of the radial glia fibers is surrounded by a black dotted line. (D) In the matrix zone, between P2 and P3 neuromeres, an aggregation of Pax6$^-$ neuroepithelial cells is indicated by a black triangular arrowhead; Pax6$^+$ niches are indicated by red arrows. (E) Dorsal thalamus (Dth). (F) General view of posterior tuberal region (PTN) with reactive neuroepithelial niches at the level of P3, P4, and P5 neuromeres (indicated by black triangle arrowheads). (G) In the anterior thalamic nucleus (Ath), reactive niches of parenchymal localization with Pax6$^-$ cells are indicated by red dotted lines. (H) In the medial thalamus (Mth), a large subventricular reactive niche is outlined by a black oval. (I) The rostral part of ventral thalamus (Vth). (J) The caudal part of Vth. (K) In the anterior part of dorsal thalamus, dashed lines indicate the migration of cells from the periventricular part of Dth to the deep layers of diencephalon to Ath. (L) In the pretectal area, Pax6$^+$ cells of the pretectal (P1) neuromere are outlined by a red rectangle. Immunoperoxidase labeling of Pax6 and staining with methyl green on transversal brain sections. Scale bars: 200 μm for A, F, and K; 100 μm for B–E, G–J, and L.

with intensely labeled Pax6$^+$ cells were located below these clusters (**Figure 12C**). In the subventricular layer, a lower density of Pax6$^+$ cells was observed (**Figure 12C**). Neurons in the nucleus of the dorsal tegmentum retained high intensity Pax6 labeling after UEI (**Figure 12D** and **Additional Table 1**). In addition to the intensely labeled cells, zones of Pax6$^-$ cells forming dense, extensive clusters were observed in the periventricular region (**Figure 12D**). In the nucleus of the oculomotor III nerve, lower intensity of immunolabeling in neurons was observed in rainbow trout with UEI than in the control rainbow trout (**Figure 12D** and **Additional Table 1**). In the periventricular areas of dorsolateral tegmentum, extensive clusters of intensely labeled undifferentiated cells were observed (**Figure 12E**). In the subventricular zone of medial tegmentum, Pax6$^+$ cells formed small, intensely labeled reactive niches (**Figure 12F**). A significantly lower density of RG fibers was observed in the tegmentum than in the periventricular diencephalon (**Figure 12G**).

In the brainstem, local aggregates of small Pax6$^-$ cells, which were not observed in the intact animals, were detected after UEI (**Figure 13A**). These groups of undifferentiated cells, which we designated reactive niches, were often located along the pathways of the lateral reticular formation in the brainstem, and many cell clusters were penetrated by RG fibers (**Figure 13B**). In the periventricular area, a large number of Pax6$^+$ RG cells were observed in the region of the IX-X nerves, where numerous migrating Pax6$^-$ cells were also found (**Figure 13B**). Small, round Pax6$^-$ ependymoglial cells were identified in the lumen of the IV ventricle above the Pax6$^+$ RG layer (**Figure 13B** and **C**). The intensity of Pax6 labeling in the nucleus of the facial nerves was lower in the animals with UEI than in the control animals (**Additional Table 1**). Large periventricular zones (PVZ) with a high cell density and maximal Pax6 activity were located in the lateral part of the brainstem (**Figure 13D**). A cluster of cells with a moderate or low activity of Pax6 was observed in the subventricular zone (**Figure 13D**). In the deep layers of brainstem, a zone of Pax6$^-$ cells extended along weakly labeled RG bundles, forming fibrous guides directed to different regions of the reticular formation. Weak intensity Pax6 labeling was detected in the Mauthner cells (M-cells) (**Figure 13E**). Intensely labeled cells in the subventricular region migrated along the Pax6$^+$ RG fibers from the periventricular area (**Figure 13E**). The dorsal surface of the M-cells was close to a large cell aggregate containing both Pax6$^-$ and

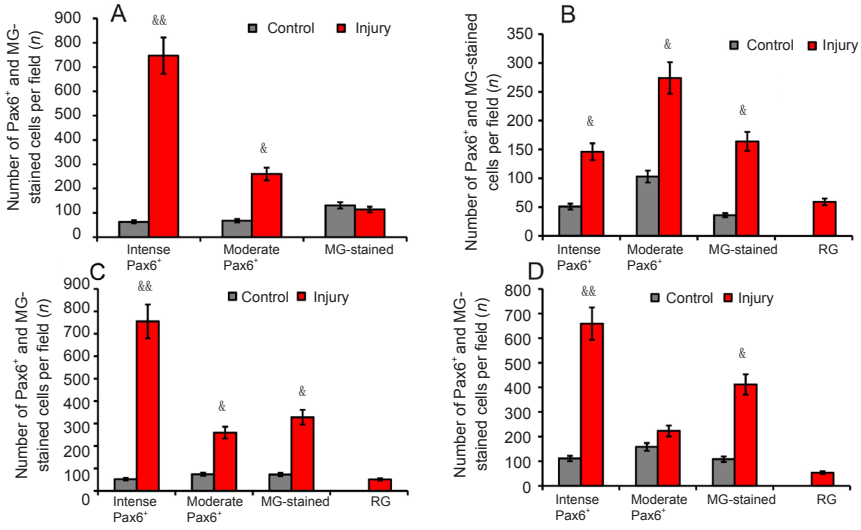

Figure 9 Density of Pax6$^+$ and Pax6$^-$ (MG-stained) cells in diencephalic nuclei of rainbow trout, *Oncorhynchus mykiss*, at 1 week after unilateral eye injury.
(A) Parvocellular preoptic nucleus. (B) Magnocellular preoptic nucleus. (C) Dorsal thalamus. (D) Ventral thalamus. One-way analysis of variance (ANOVA) followed by the Student-Newman-Keuls *post hoc* test was used to determine significant differences between control animals and animals subjected to unilateral eye injury for 1 week ($n = 5$ in each group (mean ± SD), &$P < 0.05$, &&$P < 0.01$, *vs.* control group). MG: Methyl green; RG: radial glia.

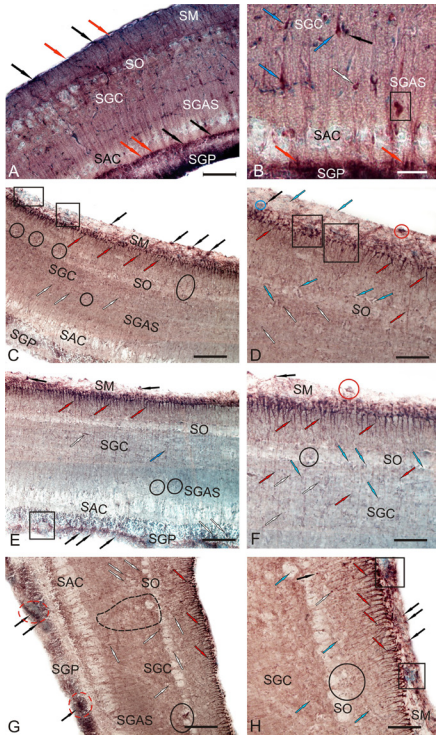

Figure 10 Localization of Pax6 in the optic tectum of intact (A and B) rainbow trout, *Oncorhynchus mykiss*, and at 1 week after unilateral eye injury (UEI; C–H).
(A) General view of Pax6-immunolabeling in the tectum, *stratum marginale* (SM), *stratum opticum* (SO), *stratum griseum centrale* (SGC), *stratum griseum et album superficiale* (SGAS), *stratum album centrale* (SAC), *stratum griseum periventriculare* (SGP) (rounded undifferentiated Pax6$^+$ cells are indicated by red arrows; oval, by black arrows). (B) Pax6 immunoreactivity in cells of deep tectal layers: bipolar cells (blue arrows), pear-shaped cells (white arrows), and a cluster of Pax6$^+$ cells (in black rectangle). (C) Pax6 immunoreactivity in the dorsal zone of tectum after UEI: intensively labeled cells and their clusters (black arrows), radial glia (red arrows), undifferentiated labeled cells of deep layers (white arrows), reactive pial niches with Pax6$^-$ cells (in black rectangles), and reactive parenchymal niches with Pax6$^-$ cells (in ovals). (D) A fragment of the dorsal zone at higher magnification: Pax6$^-$ cells are indicated by blue arrows. (E) Pax6 immunoreactivity in the medial zone of tectum after UEI: weakly labeled horizontal bipolar cells in SGC (white arrows); periventricular reactive neurogenic niche (in black rectangle). (F) A fragment of the medial zone at higher magnification: weakly Pax6-labeled cells are indicated by white arrows. (G) Pax6 immunoreactivity in the lateral zone of tectum after UEI: a large cluster of undifferentiated, weakly migrating cells (outlined by black dashed line) and reactive neurogenic niches of periventricular localization (in red dashed ovals). (H) A fragment of the lateral zone at higher magnification (see designations in A). Immunoperoxidase labeling of Pax6 and staining with methyl green on transversal brain sections. Scale bars: 200 μm for A, C, E and G; 50 μm for B, D, F, and H.

Pax6$^+$ cells (**Figure 13E**). Aggregates of Pax6$^+$ cells were also observed along the large branched outgrowths of M-cells (**Figure 13E**). In the post-injury period, RG fibers and cells appeared at the outer walls of the brainstem in contact with the pial surface (**Figure 13F**). Intense Pax6 labeling was observed in reticulospinal cells after UEI (**Figure 13G** and **Additional Table 1**). Among the large multipolar neurons of the reticular formation, we observed extensive aggregates of small undifferentiated Pax6 cells forming the reactive niches with a parenchymal localization (**Figure 13G**). The cells of the ventral oculomotor complex were intensely labeled with the Pax6 antibody (**Figure 13H** and **Additional Table 1**). Large bipolar, medium- and small-sized neurons surrounded by clusters of undifferentiated Pax6 cells were observed inside the nucleus of the abducens nerve and in adjacent regions (**Figure 13H** and **Additional Table 1**). Intense Pax6 labeling was also observed in large somatosensory neurons of the main nucleus of the trigeminal nerve and cells of the lateral reticular formation (LRF) (**Figure 13I**).

Discussion

Neurolin expression in optic nerves

IHC was performed to label Zn8, an axon regeneration factor, to describe the regenerative processes in the rainbow trout optic nerves. Previously, in studies on goldfish with different levels of nerve injury, Zn8 was shown to be involved in the process of optic nerve regeneration (Parrilla et al., 2009, 2012, 2013). In the IHC study of rainbow trout, we also detected the localization of Zn8 on the damaged side and in the contralateral optic nerve 1 week after UEI. The Zn8 axon regeneration factor was identified in the goldfish optic nerve on days 15 to 30 post-injury (Parrilla et al., 2013). During this period, Zn8 was mainly located in regenerating axons. The maximum number of regenerating axons was located in the growing edge close to the chiasm and in the mature regions of the ONH (Parrilla et al., 2013).

In our studies on rainbow trout, a few Zn8$^+$ astrocytes, forming pairs and/or small clusters of reactive cells, were identified in the contralateral nerve 1 week after the traumatic UEI. Simultaneously, we observed Zn8$^+$ regenerating

axons in the contralateral nerve. A quantitative assessment of the ratio of $Zn8^+$ cells in the contralateral nerve in various optic nerve regions showed an insignificant difference in the numbers of cells in the ONH and IOS, but more cells were observed in the proximal and distal parts of the optic nerve. Among all glial cells identified in the optic nerve after traumatic injury, a significant population comprised $Pax2^+$ astrocytes (Pushchina et al., 2018). According to the results of our observations, Pax2 immunolabeling was detected both in glial cell nuclei and in a heterogeneous population of astrocytes in the contralateral optic nerve of rainbow trout, which we divided into three main groups (Pushchina et al., 2018). Consistent with the commonly used classification (Parrilla et al., 2009), small, round $Pax2^+$ cells represent a population of reactive astroblasts, oval $Pax2^+$ cells displaying different degrees of elongation correspond to reactive astrocytes, and medium- or large-sized narrow bipolar $Pax2^+$ cells correspond to the migrating populations of astrocytes, all of which were observed after UEI in rainbow trout (Pushchina et al., 2018). The morphological and dimensional parameters of $Pax2^+$ cells were significantly different from the parameters of $Zn8^+$ cells, and thus we hypothesized that $Pax2^+$ and $Zn8^+$ cells represent different populations of glial cells in the rainbow trout optic nerve. We detected $Zn8^+$ regenerating axons in many areas of the contralateral nerve. Thus, the results of studies on rainbow trout indicate that glial cells and regenerating fibers expressing the Zn8 axon regeneration factor appear in the contralateral nerve 1 week after UEI.

The numbers of $Zn8^+$ cells and nuclei in the injured optic nerve essentially exceeded their numbers on the contralateral side. We identified $Zn8^+$ cells, and the morphological parameters are presented in **Table 1**. Additionally, we observed a large number of immunolabeled subcellular elements, the sizes of which are smaller than the usual size of the cell soma; thus, glial cell nuclei were referred to as subcellular elements. In **Figure 2B**, the population of $Zn8^+$ cells and subcellular elements is indicated by different colors (white and gray, respectively). Data from this study indicate the active participation of astrocytes in the regeneration of the rainbow trout optic nerve and the appearance of growing axons expressing Zn8 at 1 week after UEI.

Expression of Pax6 in rainbow trout brain

An IHC analysis of Pax6 localization was performed in the centers of the trout brain where the direct connections to the retina had previously been described in fish (Nortcutt, 2008): the diencephalon and optic tectum. We hypothesized that the activation of constitutive neurogenic niches and the appearance of reactive niches would be most pronounced in these areas in response to UEI. According to recent studies, progenitor cells possessing the properties of neural stem cells are present in various areas of the fish brain, such as the telencephalon, retina, midbrain, cerebellum, and spinal cord (Than-Trong and Bally-Cuif, 2015). Radial glial cells, which are the main source of long-term constitutively active and/or activated precursors characterized by high heterogeneity, including neuroepithelial progenitors, were observed in the same centers of the fish brain in previous studies (Menuet et al., 2005; Ito et al., 2010). We investigated the trout telencephalon as a center that does not have direct retinal inputs in the fish brain. The medulla oblongata is considered the most remote region from the damage zone, particularly the periventricular region, the medial and lateral reticular formation zones, the nucleus of the cranial nerves, and the pial region.

Telencephalon

According to Wullimann (1998), the retina does not form direct connections to the telencephalon in fish. However, based on the data describing the involvement of the pallial proliferative zone in reparative neurogenesis in zebrafish (Kishimoto et al., 2012), we investigated Pax6 immunolocalization in the telencephalon of control rainbow trout and those with UEI. A study of Pax6 immunolocalization in the control animals showed the presence of two levels (intense and moderate) of Pax6 immunolabeling. A much greater number of moderately labeled cells than intensely labeled cells were observed in the Dd and Dl zones.

After injury, intense Pax6 labeling was detected in reactive neurogenic niches located in the pallial proliferative Dd zone. In this area of the trout telencephalon, we did not observe $Pax6^+$ RG, but the immunolabeling of periventricular cells in the pallial zone indicates a significant increase in the number of $Pax6^+$ cells in neuroepithelial neurogenic niches. Neuroepithelial cells mainly exhibited nuclear Pax6 staining. Our data correspond to the results from zebrafish, where no typical RG were detected in the dorsal pallium, but glial precursors that are capable of symmetric (gliogenic) and asymmetric (neurogenic) division were observed (Than-Trong and Bally-Cuif, 2015). The main pool of dorso-medial progenitors of RG in zebrafish is located at the border between Dm and Dd. However, we did not reveal morphologically heterogeneous cells that would correspond to the population of RG precursors in similar zones in adult rainbow trout.

Reactive $Pax6^+$ neurogenic niches with a periventricular and subventricular localization, as well as RG fibers along which $Pax6^+$ and $Pax6^-$ cells migrated, were detected in Dl after UEI. In contrast to Dd and Dm, RG cells were observed in Dl after the injury. Dl of the zebrafish pallium is a region in which lateral RG precursors are located (Than-Trong and Bally-Cuif, 2015). According to recent data (Dirian et al., 2014), a pool of lateral neuroepithelial cells are located in Vl in zebrafish. In Dl and Vl of the rainbow trout telencephalon, we observed an intensive response from neuroepithelial cells expressing Pax6, as well as the RG after UEI. RG fibers were clearly observed extending from the surface to the deep layers of Dl and Vl. Local aggregates of RG, the fibers of which extended into the deep layers of the subpallium from separate reactive niches, were also observed in Vv after the injury.

Thus, after UEI, we observed the reactivation of constitutive neurogenic niches, the cells of which were intensely labeled with the Pax6 antibody, increased Pax6 expression in neuroepithelial cells, and the appearance of numerous reactive $Pax6^+$ domains in the pallial and subpallial proliferative zones of the trout telencephalon.

The enzyme immunoassay showed a 33% increase in the amount of the Pax6 protein in rainbow trout brain after UEI compared to the level of Pax6 in the control animals. These data are consistent with the results of IHC labeling for Pax6

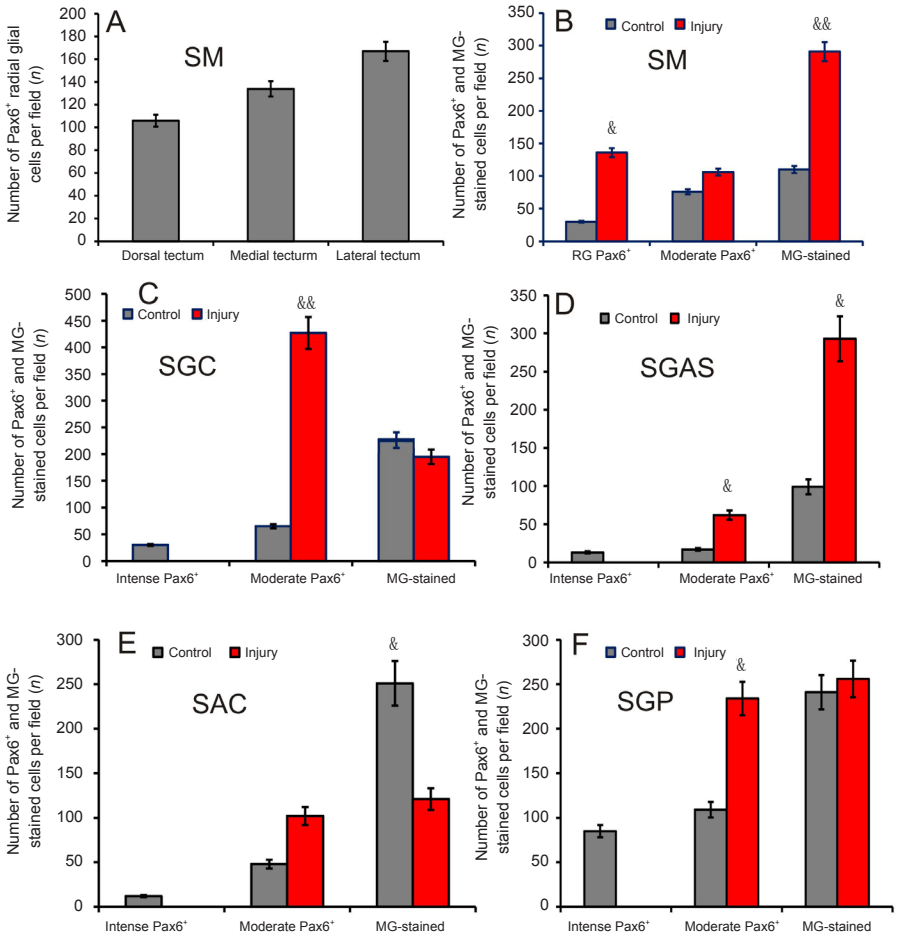

Figure 11 Number of Pax6$^+$ cells, methyl green (MG)-stained cells and radial glial cells in the tectum of intact trout and 1 week after unilateral eye injury (UEI).
(A) Number of Pax6$^+$ radial glial cells in the *stratum marginale* (SM) of the dorsal, medial, and lateral zones of tectum 1 week after UEI. (B) Number of Pax6$^+$ radial glia cells, moderately Pax6-labeled cells, and Pax6$^-$ cells in the SM of tectum. (C) *Stratum griseum centrale* (SGC) (see designations in B). (D) S*tratum griseum et album superficiale* (SGAS). (E) *Stratum album centrale* (SAC). (F) *Stratum griseum periventriculare* (SGP). (B–F) Data are expressed as the mean ± SD (n = 5 in each group); one-way analysis of variance (ANOVA) followed by the Student-Newman-Keuls *post hoc* test was used to determine significant difference between control animals and animals subjected to UEI for 1 week. &P < 0.05, &&P < 0.01, *vs.* control group.

in brain sections and were explained by the appearance of reactive niches and the reactivation of constitutive neuroepithelial niches in response to traumatic injury of the optic nerve. Thus, a neurogenic response developed in the proliferative zones of the trout telencephalon after UEI (Pushchina et al., 2016a), and the number of reactive neurogenic niches containing Pax6$^-$expressing cells increased.

In experiments in which the zebrafish telencephalon was damaged, activation of the RG in the telencephalon occurred between days 2–3 and 7 post-injury (Kizil et al., 2012; Schmidt et al., 2013). On day 21 post-injury, HuCD$^+$ cells, which are neurons that form as a result of the repair process, were detected in the damaged area of the zebrafish telencephalon (Kroehne et al., 2011). Different RG markers highlight different proportions of RG re-entering division upon lesion (*e.g.*, an important reactivation of her4$^+$ cells, some reactivation of S100b2$^-$ or BLBP$^+$ cells, and no reactivation of AroB$^+$ cells (Kroehne et al., 2011; Marz et al., 2011; Baumgart et al., 2012; Diotel et al., 2013)), suggesting the existence of subpopulations of RG with different functions and/or sensitivity to the repair process. Some silent RG upregulate a quiescence-promoting factor Id1, suggesting an active refractory response to reactivation that may be used to preserve part of the pool of neural stem cells (Schmidt et al., 2014). In addition to RG, the proliferation of pallial nonglial "transit amplifying"-like progenitors increases after lesioning (Marz et al., 2011; Baumgart et al., 2012), suggesting that progenitor recruitment is possible directly at a level of downstream of neural stem cells. The question of whether this differential recruitment is a general phenomenon or is dictated by the type or extent of the lesion remains unresolved. Moreover, researchers have not determined which cellular hierarchies are involved in the neuronal regeneration process and, possibly, in the replenishment process in germinative zones following recruitment for repair.

The properties of RG are modified by damage to the parenchymal part of the telencephalon (Than-Trong and Bally-Cuif, 2015). The precursors of regenerating neurons migrate to the damaged area, which is located much deeper in the parenchyma than the region in which adult neurons are located. The proliferative zones, which are activated during the repair process, may originate from another topographical domain (as mainly observed in the case of small-sized lesions, for example, when RG in the medial and dorsal domains are reactivated in a lesion in the central pallium (Baumgart et al., 2012; Kishimoto et al., 2012)). Although this hypothesis has not been formally validated, these observations show that the neuronal subtypes that develop from the radial glia and are activated in response to a lesion may differ from the neuronal subtypes produced during constitutive neurogenesis.

Diencephalon

Pax6 immunolabeling has been observed in the periventricular diencephalon of zebrafish (Wullimann and Muller,

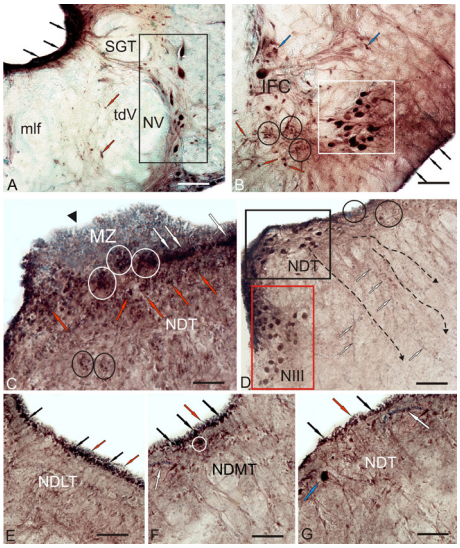

Figure 12 Localization of Pax6 in the brainstem of intact (A, B) trout, *Oncorhynchus mykiss*, and at 1 week after unilateral eye injury (UEI) (C–G).

(A) In the nucleus of trigeminal nerve (NV) (outlined by black rectangle), Pax6-labeled neurons of the periventricular region are indicated by black arrows; moderately Pax6-labeled cells of the interfascicular area are pointed by red arrows; tdV is the descending tract of the trigeminal nerve; SGT is the secondary gustatory tract; and mlf is medial longitudinal fasciculus. (B) In the nucleus of abducens nerve (VI) (in a white square), constitutive neurogenic niches are outlined by black circles; subpial radial glia, by black arrows; moderately Pax6-labeled cell, by blue arrows; IFC is interfascicular cell. (C) Pax6 immunoreactivity in the tegmental area after UEI: conglomerates of undifferentiated ependymoglial Pax6$^-$ cells of the matrix zone (MZ) in the region of mesencephalic neuromere (black triangular arrowhead); reactive subventricular niches (in white oval); Pax6$^+$ cells in the subventricular area (white arrows) and in tegmental parenchyma (red arrows); reactive niches of parenchymal localization (in black ovals). (D) Pax6-immunoreactivity in dorsal tegmental nuclei (NDT, in black rectangle), in the nucleus of the oculomotor nerve (NIII, in red rectangle), and in reactive niches (in ovals). (E) Periventricular areas of dorso-lateral tegmentum (NDLT). (F) Periventricular areas of medial tegmentum (NDMT). (G) In periventricular areas of dorsal tegmentum: Pax6$^+$ periventricular cells (black arrows), Pax6$^-$ cells (red arrows), blood vessels (white arrows), and Pax6$^+$ neurons of tegmentum (blue arrow). Immunoperoxidase labeling of Pax6 and staining with methyl green on transversal brain sections. Scale bars: 100 μm for A, B, and D; 50 μm for C, E–G.

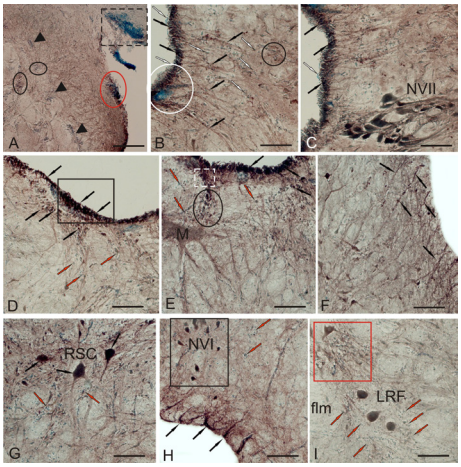

Figure 13 Localization of Pax6 in the brainstem of rainbow trout, *Oncorhynchus mykiss*, at 1 week after unilateral eye injury (UEI).

(A) Pax6$^+$ neurogenic niches (black triangular arrowheads) in the brainstem, a ventro-caudal reactive cluster located at the base of tectum (in black dashed rectangle), a subpial reactive cluster (in red oval), and reactive clusters of parenchymal localization (in black ovals). (B) Reactive neurogenic niches in periventricular and subventricular regions: Pax6$^-$ cells (white arrows), Pax6$^+$ cells (black arrows), a subventricular reactive cluster (in white oval), and a parenchymal reactive cluster (in black oval). (C) Nucleus of facial nerve (NVII). (D) Periventricular reactive neurogenic zone (in rectangle) in the lateral part of brainstem. (E) In the M-cell of brainstem; a subventricular reactive neurogenic cluster is outlined by white dashed line; larger reactive neurogenic zone is outlined by a black oval. (F) Pax6$^+$ cells and radial glial fibers (black arrows) in the subpial region of brainstem. (G) Reactive parenchymal clusters of Pax6$^-$ cells (red arrows) near reticulo-spinal cells (RSC; black arrows). (H) Pax6$^+$ neurons of the abducens nerve (NIV, in black rectangle), Pax6$^+$ radial glial cells in the subpial area (black arrows), and parenchymal neurogenic clusters (red arrows). (I) Pax6$^+$ neurons of the main nucleus of the trigeminal nerve (NV) and lateral reticular formation (LRF; in red square), surrounded by numerous Pax6$^-$ parenchymal cells. Immunoperoxidase labeling of Pax6 and staining with methyl green on transversal brain sections. Scale bars: 200 μm for A; 100 μm for B–I.

2004) and juvenile *O. masou* (Pushchina et al., 2012). The presence of Pax6$^+$ cells in the periventricular area of juvenile fish indicates the presence of constitutive neurogenesis in these regions of the brain. In the nuclei of the trout diencephalon, Pax6 immunoreactivity was detected in the preoptic area and the periventricular nuclei of thalamus in the intact animals, but few labeled cells were observed in the intact animals. In trout with a damaged optic nerve, significant structural rearrangements, the appearance of Pax6$^+$ radial glia, and the reactivation of constitutive neuroepithelial neurogenic niches in the region of the prosencephalic P1, P2 and P3 neuromeres were observed in the periventricular diencephalic nuclei. In adult zebrafish, constitutive RG were detected in the preoptic area, epithalamus, dorsal and ventral thalamus, posterior tubercle, the dorsal, ventral and caudal regions of hypothalamus, nuclei of the diencephalon and the pretectum of the diencephalon (Than-Trong and Bally-Cuif, 2015). The RG in these areas of the zebrafish diencephalon express various markers, such as GFAP, BLBP, or AroB (Menuet et al., 2005). The presence of constitutive RG in the diencephalon of different age groups of *O. masou,* including adults, was reported in our previous studies (Pushchina et al., 2013). After the traumatic injury of the ON, an essential increase in the number of Pax6$^+$ cells was revealed in the region of germinative zones of diencephalon and in the adjacent subventricular regions in the periventricular nuclei of the trout diencephalon. Pax6$^+$ cells with the RG phenotype were detected in the areas of prosencephalic neuromeres (POm, Dth and Vth) after UEI. In the area of the constitutive neurogenic niches adjacent to P2 and P3 neuromeres, Pax6$^-$ neuroepithelium appeared in the region of germinative zones of the dorsal and ventral thalamus and the postero-tuberal region after the injury. Intensely labeled Pax6$^+$ local neurogenic zones were found in the same areas of the injured animals, but not the control animals. We designated these neurogenic areas surrounding the fasciculus retroflexus, which is located in the postero-tuberal area and in the ventral thalamus, the reactive niches that arise in response to UEI. We identified Pax6$^-$ undifferentiated cell clusters in the deep regions of the diencephalon, which were absent in the control animals. We also classified these structures as reactive neurogenic niches with a parenchymal localization. These clusters of cells were detected in the ventral thalamus, pretectal and preglomerular regions. Based on our observations, reactive neurogenesis occurs in the diencephalic nuclei of trout in response to UEI.

Thus, we recorded the following observations in the trout diencephalon after UEI: (1) the appearance of reactive Pax6$^+$

and Pax6$^-$ neurogenic niches with a periventricular and parenchymal localization; (2) the appearance of Pax6$^+$ RG in the POm, Dth, and Vth; (3) an increase in the number of intensely labeled Pax6$^+$ cells in the POp, POm, Dth, and Vth; (4) an increase in the number of moderately labeled Pax6$^+$ cells in the PO and Dth; and (5) an increase in the number of Pax6$^+$ cells in the POm, Dth, and Vth. Thus, in rainbow trout, UEI leads to a neurogenic response in the visual centers of thalamus and the preoptic region and to the formation of numerous reactive niches that have apparently a neuroepithelial origin and are located in the region of the subventricular zone and in the deep parenchymal regions of the diencephalon.

A study of diencephalic nuclei, particularly the preoptic region, the thalamic ventricle and the hypothalamus performed by labeling sections with BrdU and PCNA showed the presence of constitutive neurogenesis in these areas of the brain in zebrafish (Pellegrini et al., 2007) and *O. masou* (Pushchina et al., 2013). Pax6$^+$, tyrosine hydroxylase (TH)$^+$, and gamma-aminobutyric acid (GABA)$^+$ neurons were identified in the periventricular diencephalon of 2-year-old *O. masou* (Pushchina et al., 2012, 2013), and 5-hydroxytryptamine (5-HT)$^+$ neurons were observed in the paraventricular organ in the zebrafish hypothalamus (Grandel et al., 2006). However, the origin of these distinct neuronal populations remains unclear, since BrdU labels not only RG but also non-radial progenitors (Pellegrini et al., 2007). The only exception is the paraventricular organ, in which most of the proliferating cells are RG, suggesting that the RG are a major source of serotonergic neurons in the paraventricular organ (Perez et al., 2013).

Optic tectum

The tectum is the largest area of the fish brain that receives directed retinal inputs (Wullimann, 1998). In the control animals, Pax6 immunoreactivity was detected in cells of different layers of the optic tectum. We detected two levels of intensity of Pax6 immunolabeling in neurons of different morphological types: high and moderate. A small number of intensely labeled Pax6$^+$ RG in the marginal layer were observed in the control animals. We associated the presence of RG in the marginal layer of the tectum with constitutive neurogenesis. After UEI, the number of RG increased substantially in the dorsal, medial, and lateral zones, reaching the maximum level in the latero-caudal region of the tectum (**Figure 11A**). Cells with the RG morphology were the predominant type of intensely labeled Pax6$^+$ cells observed after UEI.

In the intact animals, we also identified a small number of similar cells in the MS, as well as separate, intensely labeled differentiated cells displaying a cytoplasmic localization of Pax6 in the deep layers (SGC, SGAS, and SAC) of the tectum. Similar Pax6 immunolabeling was also observed in projection neurons from other parts of the rainbow trout brain; however, we did not observe Pax6 labeling in the differentiated cells of the tectum after UEI. Intense Pax6 immunolabeling was detected in separate undifferentiated cells located in the deep tectal layers after UEI. A significant increase in the number of Pax6$^+$ radial glia was observed in the MS, which contains both RG cell bodies and their processes, and Pax6$^+$ radial glia were traced into the deep layers of the tectum. In the MS and SGAS, we detected a significant increase in the number of Pax6$^-$ undifferentiated cells in the reactive neurogenic niches after UEI. Superficial neurogenic Pax6 niches were detected in the MS; Pax6$^-$ niches with a parenchymal localization were identified in the SGAS. Significant increases in the numbers of moderately and weakly labeled Pax6$^+$ undifferentiated cells migrating along the RG fibers were observed in the SGC, SGAS, and SGP after injury. In general, the pattern of Pax6 immunolabeling after UEI indicates significant changes in Pax6 expression in the tectum, particularly the localization in RG and undifferentiated cells of the deep layers. Thus, we postulate that the tectum is one of the main zones of the brain that participates in repair in response to a traumatic UEI.

Regarding progenitor cells and the constitutive growth of the brain, the organization of the fish optic tectum is very similar to the organization of the retina, as the marginal zone contains proliferating cells. The marginal zone of the retina is responsible for the addition of neurons throughout the life-cycle, while the tectal RG are not proliferating, according to Alunni et al. (2010) and Ito et al. (2010). As shown in our recent study, RG located in MS of the rainbow trout tectum are labeled with PCNA after UEI (Pushchina et al., 2016b). Thus, the tectal RG may correspond to the Muller glial cells and represent an additional source of precursors that are activated after injury to promote recovery and, possibly, the production of neurons at a low rate under physiological conditions. To date, this issue has not yet been investigated.

Medulla oblongata

In the control animals, IHC labeling of Pax6 was detected in the paraventricular area, as well as in the nuclei of the cranial nerves and in some projection neurons of the reticular formation. These areas of the brainstem in the control animals were characterized by high intensity Pax6 labeling. After UEI, Pax6-immunoreactive niches with parenchymal, pial and subpial localizations were in the medulla oblongata of injured animals, but not in control animals.

In the rainbow trout brainstem, the reactivation of constitutive neurogenic niches with periventricular localization, including Pax6$^-$ and Pax6$^+$ cells, was detected after UEI. The reactive neurogenic niches were located in the outer layers of the medulla oblongata and contained both Pax6$^-$ and Pax6$^+$ cells. Very high intensity Pax6 labeling was observed in these reactive neurogenic niches. In addition to the neurogenic niches, single intensely labeled Pax6$^+$ neurons and RG fibers were detected in the outer subpial layers of the medulla oblongata. This localization of Pax6$^+$ cells and RG in areas of adult neurogenesis was not revealed in the control animals and is considered a reaction to UEI. Another feature of the repair response in the medulla oblongata was the appearance of numerous reactive Pax6$^-$ neurogenic niches with parenchymal localization, which were absent in the control animals. We observed a slight decrease in the intensity of Pax6 immunolabeling in large projection cells of the reticular formation and nuclei of the cranial nerves in the medulla oblongata of injured animals compared to the control animals. Thus, numerous reactive neurogenic niches were observed in the secondary proliferative areas and

brainstem parenchyma, and constitutive neurogenic niches in the periventricular region were activated in the medulla oblongata after UEI.

In experiments in which the zebrafish spinal cord was damaged, and the proliferation of ependymoglial cells in the central canal of the spinal cord was observed within 2 weeks after injury (Reimer et al., 2008). The generation of motor neurons from activated Olig2$^+$ progenitors was documented using green fluorescent protein (GFP) as a tracer in olig2 : gfp transgenics, together with BrdU labeling (Reimer et al., 2008). Thus, the subsequent fate of these progenitors, including the appearance of oligodendrocytes, was modified, and new motor neurons appeared in response to injury. The more dorsally located ependymoglial cells expressed the transcription factors Pax6 and Nkx6.1, and started to generate V2 interneurons upon activation in response to traumatic injury (Kuscha et al., 2012b).

In our studies, we did not directly damage the brainstem. However, numerous reactive niches of a neuroepithelial/ependymoglial origin appeared in the brainstem and the tegmental matrix zones near the IV ventricle after UEI. We identified numerous neurogenic niches with a parenchymal localization in the medullary reticular formation and cranial nerve nuclei, as well as in the subpial areas of brainstem. The fates of other activated ependymoglial cells in zebrafish, *e.g.*, those expressing *shh* ventrally or those located in the alar plate, have not yet been traced (Reimer et al., 2009). Other neuronal subtypes, including Pax2$^+$ interneurons and spinal serotonergic neurons, also regenerate after a spinal cord injury (Kuscha et al., 2012a, b). To date, the regenerating spinal cord is the only model of the zebrafish CNS that considers neuromodulatory factors: dopamine synthesized by descending projection neurons is involved in the regeneration of V2 interneurons (Reimer et al., 2013). The fates of ependymoglial cells in the spinal cord after injury are not similar. An increase in the number of these cells in response to damage indicates symmetric gliogenic divisions (Reimer et al., 2009). The questions regarding what type of cell division characterizes the generation of neurons and how this division is controlled at the level of individual cells or their populations remain unresolved.

In our studies on juvenile *Oncorhynchus masou*, we detected a population of TH$^+$ and GABA$^+$ cells located in the medullary column of the reticular formation in the medulla oblongata (Pushchina et al., 2013). TH and GABA were also identified in different periventricular regions of the brain at the bottom of the IV ventricle, which simultaneously contained PCNA$^+$ proliferating cells (Pushchina et al., 2013). Thus, according to the data obtained from studies of the zebrafish spinal cord and the results of our own observations, the population of catecholaminergic and GABA-ergic neurons in the brainstem and the diencephalic matrix zones of *Oncorhynchus masou* juveniles clearly indicates that some neurotransmitters participate in constitutive neurogenesis in the fish brain. The reactive niches including ependymoglial cells that appear after UEI in rainbow trout confirm the reparative neurogenic response in the rainbow trout brainstem that is considered a compensatory physiological reaction of the rainbow trout brain to injury.

Conclusions

According to the IHC staining of the adult rainbow trout, both glial cells and regenerating fibers of the contralateral optic nerve express axon regeneration factor Zn8 1 week after UEI. The comparative analysis of the distribution of Zn8$^+$ cells and their percentages in different areas of contra- and ipsilateral optical nerves revealed a significantly greater number of Zn8$^+$ cells in the optical nerve head and intraorbital segment on the damaged side at 1 week post-injury. The number of Zn8$^+$ cells in the proximal and distal parts of the damaged optic nerve essentially exceeds the number observed on the contralateral side. These data indicate the active involvement of Zn8$^+$ astrocytes in the regeneration of the rainbow trout optic nerve, as well as the appearance of growing axons expressing Zn8 at 1 week post-injury. Based on the ELISA data, the concentration of the Pax6 protein is significantly increased in the rainbow trout brain after UEI compared to the control animals. An IHC analysis of Pax6 localization was performed in the centers of the rainbow trout brain that participate in direct connections to the retina, as described in previous studies using fish: nuclei of the diencephalon and optic tectum. In these areas of the rainbow trout brain, the reactivation of constitutive neurogenesis and the appearance of reactive neurogenic niches are presumed to occur in response to UEI. We observed Pax6$^+$ RG in the same centers of the rainbow trout brain; RG are the main source of long-term constitutively active and/or activated precursors that are characterized by high heterogeneity, including neuroepithelial progenitors. Numerous reactive Pax6$^+$ domains appeared in the pallial and subpallial proliferative zones of the trout telencephalon. UEI leads to a neurogenic response in the visual centers of the thalamus and the preoptic region of the trout diencephalon and the formation of numerous reactive niches that apparently have a neuroepithelial origin and are located in the area of the subventricular zone and in the deep parenchymal regions. The pattern of Pax6 immunolabeling in the tectum was altered after UEI, particularly the localization of RG in the surface and periventricular layers and undifferentiated cells of the deep tectal layers. We postulate that the tectum is one of the main centers of the brain participating in the repair response after UEI. The appearance of reactive niches that include ependymoglial cells after UEI in rainbow trout confirms the presence of a reparative neurogenic response in the rainbow trout brainstem and is considered a compensatory physiological reaction of the brain to trauma.

Author contributions: *Study design, animal model preparation, immunohistochemistry implement, experimental data analysis, and paper writing: EVP; paper writing and critical revision of the paper for intellectual content: AAV. Both authors approved the final version of this paper.*
Conflicts of interest: *No competing financial interests exist.*
Financial support: *This work was supported by the President of the Russian Federation (grant No. MD-4318.2015.4; to EVP) and by the Far East Branch of the Russian Academy of Sciences within the Program for Basic Research for 2015–2017 (grant No. 15-I-6-116; section III; to AAV and EVP). The funding bodies played no role in the study design, in the collection, analysis and interpretation of data, in the writing of the paper, and in the decision to submit the paper for publication.*
Institutional review board statement: *All experimental manipulations with animals were carried out in accordance with the rules established by the National Center for Marine Biology, the Resource Center of the National Scientific Center of Marine Biology (NSCMB), Far Eastern Branch Russian*

of the Russian Academy of Science (FEB RAS), and by the Commission on Biomedical Ethics of National Scientific Center of Marine Biology of the Far Eastern Branch of the Russian Academy of Sciences (approval No. 3) on February 25, 2018.

Data sharing statement: *Datasets analyzed during the current study are available from the corresponding author on reasonable request.*

Plagiarism check: *Checked twice by iThenticate.*

Peer review: *Externally peer reviewed.*

Open peer reviewers: *Steven Levy, MD Stem Cells, Ophthalmology, USA; Chaoran Ren, Jinan University, China.*

Additional files:

Additional Table 1: *Morphometric parameters of $Zn8^+$ and $Zn8^-$ cells in the optic nerve of rainbow trout, Oncorhynchus mykiss, at 1 week after unilateral eye injury.*

Additional file 1: *Open peer review reports 1 and 2.*

References

Alunni A, Hermel JM, Heuze A, Bourrat F, Jamen F, Joly JS (2010) Evidence for neural stem cells in the medaka optic tectum proliferation zones. Dev Neurobiol 70:693-713.

Baumgart EV, Barbosa JS, Bally-Cuif L, Gotz M, Ninkovic J (2012) Stab wound injury of the zebrafish telencephalon: a model for comparative analysis of reactive gliosis. Glia 60:343-357.

Becker CG, Becker T (2007) Growth and pathfinding of regenerating axons in the optic projection of adult fish. J Neurosci Res 85:2793-2799.

Diotel N, Vaillant C, Gabbero C, Mironov S, Fostier A, Gueguen MM, Anglade I, Kah O, Pellegrini E (2013) Effects of estradiol in adult neurogenesis and brain repair in zebrafish. Horm Behav 63:193-207.

Dirian L, Galant S, Coolen M, Chen W, Bedu S, Houart C, Bally-Cuif L, Foucher I (2014) Spatial regionalization and heterochrony in the formation of adult pallial neural stem cells. Dev Cell 30:123-136.

García DM, Koke JR (2009) Astrocytes as gate-keepers in optic nerve regeneration – a mini-review. Comp Biochem Physiol A Mol Integr Physiol 152:135-138.

Gerber JK, Richter T, Kremmer E, Adamski J, Höfler H, Balling R, Peters H (2002) Progressive loss of PAX9 expression correlates with increasing malignancy of dysplastic and cancerous epithelium of the human oesophagus. J Pathol 197:293-297.

Grandel H, Kaslin J, Ganz J, Wenzel I, Brand M (2006) Neural stem cells and neurogenesis in the adult zebrafish brain: origin, proliferation dynamics, migration and cell fate. Dev Biol 295:263-277.

Heins N, Malatesta P, Cecconi F, Nakafuku M, Tucker KL, Hack MA, Chapouton P, Barde YA, Götz M (2002) Glial cells generate neurons: the role of the transcription factor Pax6. Nat Neurosci 5:308-315.

Ito Y, Tanaka H, Okamoto H, Ohshima T (2010) Characterization of neural stem cells and their progeny in the adult zebrafish optic tectum. Dev Biol 342:26-38.

Kishimoto N, Shimizu K, Sawamoto K (2012) Neuronal regeneration in a zebrafish model of adult brain injury. Dis Model Mech 5:200-209.

Kizil C, Kaslin J, Kroehne V, Brand M (2012) Adult neurogenesis and brain regeneration in zebrafish. Dev Neurobiol 72:429-461.

Kleinjan DA, Bancewicz RM, Gautier P, Dahm R, Schonthaler HB, Damante G, Seawright A, Hever AM, Yeyati PL, van Heyningen V, Coutinho P (2008) Subfunctionalization of duplicated zebrafish pax6 genes by cis-regulatory divergence. PLoS Genet 4:e29.

Kroehne V, Freudenreich D, Hans S, Kaslin J, Brand M (2011) Regeneration of the adult zebrafish brain from neurogenic radial glia-type progenitors. Development 138:4831-4841.

Kuscha V, Barreiro-Iglesias A, Becker CG, Becker T (2012a) Plasticity of tyrosine hydroxylase and serotonergic systems in the regenerating spinal cord of adult zebrafish. J Comp Neurol 520:933-951.

Kuscha V, Frazer SL, Dias TB, Hibi M, Becker T, Becker CG (2012b) Lesion-induced generation of interneuron cell types in specific dorsoventral domains in the spinal cord of adult zebrafish. J Comp Neurol 520:3604-3616.

Marz M, Schmidt R, Rastegar S, Strahle U (2011) Regenerative response following stab injury in the adult zebrafish telencephalon. Dev Dyn 240:2221-2231.

Menuet A, Pellegrini E, Brion F, Gueguen MM, Anglade I, Pakdel F, Kah O (2005) Expression and estrogen-dependent regulation of the zebrafish brain aromatase gene. J Comp Neurol 485:304-320.

Ninkovic J, Pinto L, Petricca S, Lepier A, Sun J, Rieger MA, Schroeder T, Cvekl A, Favor J, Götz M (2010) The transcription factor Pax6 regulates survival of dopaminergic olfactory bulb neurons via crystallin αA. Neuron 68:682-694.

Northcutt RG (2008) Forebrain evolution in bony fishes. Brain Res 75:191-205.

Parrilla M, Lillo C, Herrero-Turrión MJ, Arévalo R, Aijón J, Lara JM, Velasco A (2012) Characterization of Pax2 expression in the goldfish optic nerve head during retina regeneration. PLoS One 7:e32348.

Parrilla M, Lillo C, Herrero-Turrion MJ, Arévalo R, Lara JM, Aijón J, Velasco A (2009) Pax2 in the optic nerve of the goldfish, a model of continuous growth. Brain Res 1255:75-88.

Parrilla M, Lillo C, Herrero-Turrión MJ, Arévalo R, Aijón J, Lara JM, Velasco A (2013) Pax2+ astrocytes in the fish optic nerve head after optic nerve crush. Brain Res 1492:18-32.

Pellegrini E, Mouriec K, Anglade I, Menuet A, Le Page Y, Gueguen MM, Marmignon MH, Brion F, Pakdel F, Kah O (2007) Identification of aromatase-positive radial glial cells as progenitor cells in the ventricular layer of the forebrain in zebrafish. J Comp Neurol 501:150-167.

Perez MR, Pellegrini E, Cano-Nicolau J, Gueguen MM, Menouer-Le Guillou D, Merot Y, Vaillant C, Somoza GM, Kah O (2013) Relationships between radial glial progenitors and 5-HT neurons in the paraventricular organ of adult zebrafish - potential effects of serotonin on adult neurogenesis. Eur J Neurosci 38:3292-3301.

Pushchina EV, Obukhov DK, Varaksin AA (2013) Features of adult neurogenesis and neurochemical signaling in the Cherry salmon Oncorhynchus masou brain. Neural Regen Res 8:13-23.

Pushchina EV, Varaksin AA, Obukhov DK (2016a) Reparative neurogenesis in the brain and changes in the optic nerve of adult trout Oncorhynchus mykiss after mechanical damage of the eye. Rus J Dev Biol 47:11-32.

Pushchina EV, Shukla S, Varaksin AA, Obukhov DK (2016b) Cell proliferation and apoptosis in optic nerve and brain integration centers of adult trout Oncorhynchus mykiss after optic nerve injury. Neural Regen Res 11:578-590.

Pushchina YeV, Obukhov DK, Varaksin AA (2012) Neurochemical markers of cells of the periventricular brain area in the masu salmon Oncorhynchus masou (Salmonidae). Rus J Dev Biol 43:35-48.

Pushchina EV, Varaksin AA, Obukhov DK (2018) The Pax2 and Pax6 transcription factors in the optic nerve and brain of trout Oncorhynchus mykiss after a mechanical eye injury. Rus J Dev Biol 49:294-323.

Reimer MM, Kuscha V, Wyatt C, Sorensen I, Frank RE, Knuwer M, Becker T, Becker CG (2009) Sonic hedgehog is a polarized signal for motor neuron regeneration in adult zebrafish. J Neurosci 29:15073-15082.

Reimer MM, Norris A, Ohnmacht J, Patani R, Zhong Z, Dias TB, Kuscha V, Scott AL, Chen YC, Rozov S, Frazer SL, Wyatt C, Higashijima S, Patton EE, Panula P, Chandran S, Becker T, Becker CG (2013) Dopamine from the brain promotes spinal motor neuron generation during development and adult regeneration. Dev Cell 25:478-491.

Reimer MM, Sorensen I, Kuscha V, Frank RE, Liu C, Becker CG, Becker T (2008) Motor neuron regeneration in adult zebrafish. J Neurosci 28:8510-8516.

Schmidt R, Strahle U, Scholpp S (2013) Neurogenesis in zebrafish - from embryo to adult. Neural Dev 8:3.

Schmidt R, Beil T, Strahle U, Rastegar S (2014) Stab wound injury of the zebrafish adult telencephalon: a method to investigate vertebrate brain neurogenesis and regeneration. J Vis (90):e51753.

Stoykova A, Gruss P (1994) Roles of Pax-genes in developing and adult brain as suggested by expression patterns. J Neurosci 14:1395-1412.

Than-Trong E, Bally-Cuif L (2015) Radial glia and neural progenitors in the adult zebrafish central nervous system. Glia 63:1406-1428.

Thompson JA, Ziman M (2011) Pax genes during neural development and their potential role in neuroregeneration. J Prog Neurobiol 94:334-351.

Wullimann MF (1998) The central nervous system. In: The Physiology of Fishes (Evans DH, ed), pp245-282. Boca Raton: CRS Press.

Wullimann MF, Muller T (2004) Teleostean and mammalian forebrains contrasted: evidence from genes to behavior. J Comp Neurol 475:143-162.

P-Reviewers: Johnson T, Levy S, Ren C; C-Editor: Zhao M; S-Editor: Li CH; L-Editor: Song LP; T-Editor: Liu XL